Reversible O_2 Binding to a Dinuclear Copper(I) Complex with Linked Tris(2-pyridylmethyl)amine Units: Kinetic−Thermodynamic Comparisons with Mononuclear Analogues

Dong-Heon Lee,[†] Ning Wei,[†] Narasimha N. Murthy,[†] Zoltán Tyeklár,[†] Kenneth D. Karlin,*[,†] Susan Kaderli,[‡] Bernhard Jung,[‡] and Andreas D. Zuberbühler*[,‡]

Contribution from the Department of Chemistry, The Johns Hopkins University, Baltimore, Maryland 21218, and Institute of Inorganic Chemistry, University of Basel, CH-4056 Basel, Switzerland

Received June 13, 1995[⊗]

Abstract: The kinetics and thermodynamics of reaction of O_2 with copper(I) complexes can provide fundamental information relevant to chemical and biological systems. Using diode-array variable-temperature (180−296 K) stopped-flow kinetic methods, we report detailed information on the O_2 reactivity (in EtCN) of dicopper(I) complex $[(D^1)Cu^I_2(RCN)_2]^{2+}$ (**2a**) (R = Me or Et) [D^1 = dinucleating ligand with a $-CH_2CH_2-$ group linking two tris(2-pyridylmethyl)amine (TMPA) units at a 5-pyridyl position of each tetradentate moiety]. A comparative study of mononuclear complex $[(TMPAE)Cu(RCN)]^+$ (**1a′**) [TMPAE has a $-C(O)OCH_3$ ester substituent in the 5-position of one pyridyl group of TMPA] has been carried out. The results are compared with data from the previously investigated complex $[(TMPA)Cu(RCN)]^+$ (**1a**). The syntheses of D^1 and **2a**-$(ClO_4)_2$ are described; an X-ray structure reveals two pentacoordinate Cu(I) ions (Cu···Cu = 11.70 Å), each bound by the N_4-tetradentate and an EtCN molecule. Cyclic voltammetric data for **1a′** and **2a** are reported. At 193 K in EtCN, **2a** reacts with O_2 (Cu/O_2 = 2:1, manometry) to produce an intensely purple colored solution of adduct $[(D^1)Cu_2(O_2)]^{2+}$ (**2c**), λ_{max} = 540 nm (ϵ = 11 100 M^{-1} cm^{-1}). This peroxo−dicopper(II) species reacts with PPh_3, liberating O_2 and producing the isolatable bis-phosphine adduct $[(D^1)Cu_2(PPh_3)_2]^{2+}$. The kinetic investigation provides spectral characterization of transient Cu/O_2 1:1 adducts generated upon oxygenation of cold solutions of **1a′** or **2a**. $[(TMPAE)Cu(O_2)]^+$ (**1b′**) forms reversibly (λ_{max} = 415 nm) with $k_1 = (8.2 \pm 0.4) \times 10^3$ M^{-1} s^{-1} and $K_1 = k_1/k_{-1} = (284 \pm 9)$ M^{-1} at 183 K, with $\Delta H_1° = (-32 \pm 1)$ kJ mol^{-1}, $\Delta S_1° = (-127 \pm 3)$ J K^{-1} mol^{-1}. Two types of Cu(II)−O_2^- complexes form in the reaction of **2a**: a 2:1 *open* form (i.e., $[(D^1)Cu_2(O_2)(EtCN)]^{2+}$, **2b**) and a bis-$O_2$ 2:2 *open* adduct (i.e., $[(D^1)Cu_2(O_2)_2]^{2+}$, **2b′**). For the formation of **2b**, $k_1 = (1.63 \pm 0.01) \times 10^4$ M^{-1} s^{-1} and $K_1 = (2.03 \pm 0.04) \times 10^3$ M^{-1} at 183 K. Complexes **2b** and **2b′** have identical spectroscopic properties (λ_{max} = 416 nm, ϵ = 4500 M^{-1} cm^{-1}) per Cu−O_2 unit, and their rate constants are statistically related. Intermediates **1b′** and **2b** further convert into (μ-peroxo)dicopper(II) [(2 Cu):(1 O_2)] complexes. $[\{(TMPAE)Cu\}_2(O_2)]^{2+}$ (**1c′**) (λ_{max} = 532 nm, ϵ = 9380 M^{-1} cm^{-1}) forms in a second-order reaction of **1b′** with **1a′** with $K_1K_2 = (2.1 \pm 0.4) \times 10^{11}$ M^{-2} at 183 K ($\Delta H_{12}° = -77 \pm 1$ kJ mol^{-1} and $\Delta S_{12}° = -203 \pm 5$ J K^{-1} mol^{-1}), while $[(D^1)Cu_2(O_2)]^{2+}$ (**2c**) (λ_{max} = 540 nm, ϵ = 11 100 M^{-1} cm^{-1}) is generated from **2b** in an *intramolecular* reaction, with $k_2 = (3.51 \pm 0.05) \times 10^1$ s^{-1} and $k_{on} = k_1k_2/k_{-1} = (7.1 \pm 0.2) \times 10^4$ M^{-1} s^{-1} (183 K). The overall formation of **2c** is faster than for **1c′** or $[\{(TMPA)Cu\}_2(O_2)]^{2+}$ (**1c**) because of a more positive entropy of activation ($\Delta S_{on}^{‡} = (-139 \pm 3)$ J K^{-1} mol^{-1} for **2c** vs $\Delta S_{on}^{‡} = (-201 \pm 5)$ J K^{-1} mol^{-1} for **1c**). However, this significantly enhanced kinetic reactivity (for **2a** → **2c**) is not reflected by an analogous increase in thermodynamic stability. $[(D^1)Cu_2(O_2)]^{2+}$ (**2c**) is enthalpically less stable ($\Delta H_{12}° = (-34.8 \pm 0.4)$ kJ mol^{-1}) than Cu_2O_2 species **1c** and **1c′** ($\Delta H_{12}° = -81$ to -77 kJ mol^{-1}, respectively), which are formed from mononuclear precursors. There is a substantially larger overall formation entropy for **2c** [$\Delta S_{12}° = (-89.3 \pm 1.5)$ J K^{-1} mol^{-1} compared to -220 and -203 J K^{-1} mol^{-1} for **1c** and **1c′**, respectively] since Cu_2O_2 formation is an intramolecular, rather than intermolecular, process. Examination of other kinetic parameters and spectral differences provides complementary information that **2c** has a strained structure. In fact, **2c** is not the ultimate oxidation product: relief of steric constraints occurs at higher temperatures by a slow rearrangement (λ_{max} = 540 nm → λ_{max} = 529 nm) producing $\{Cu_2O_2\}_n$ oligomers containing *intermolecular* Cu−O_2−Cu bonds. A particularly stable trimer species $[\{(D^1)Cu_2(O_2)\}_3]^{6+}$ (**2d**) was characterized, with $\Delta H_3° = (-153$ kJ $mol^{-1})/3 = -51$ kJ mol^{-1} per Cu_2O_2 unit, intermediate between that seen for **2c**, **1c**, and **1c′**. Thus, (peroxo)dicopper(II) complexes formed from mononuclear precursors are the most stable, while secondary rearrangements within intramolecularly formed Cu_2−O_2 complexes with dinucleating ligands can and do occur. Comparisons are made with relevant copper−dioxygen complexes, and the chemical and biological relevance of this chemistry is discussed.

Introduction

Metal−dioxygen (O_2) interactions occur widely in biological systems,[1] at heme (porphyrin-iron) centers,[2,3] non-heme iron,[4,5] and copper enzyme active sites.[6−11] Such processes include O_2 transport, dioxygenation (i.e., incorporation of two atoms

[†] The Johns Hopkins University.
[‡] University of Basel.
[⊗] Abstract published in *Advance ACS Abstracts,* December 1, 1995.

(1) Karlin, K. D. *Science* **1993**, *261*, 701−708.
(2) Momenteau, M.; Reed, C. A. *Chem. Rev.* **1994**, *94*, 659−698.
(3) Dawson, J. H. *Science* **1988**, *240*, 433−439.
(4) Feig, A. L.; Lippard, S. J. *Chem. Rev.* **1994**, *94*, 759−805.
(5) Que, L., Jr. In *Bioinorganic Catalysis*; Reedijk, J., Ed.; Marcel Dekker, Inc.: New York, 1993; pp 347−393.

0002-7863/95/1517-12498$09.00/0

of O_2 into an organic substrate), hydroxylation by monooxygenases, and dehydrogenation of organics where the reactions are driven by the reduction of O_2 to either hydrogen peroxide or water. As dioxygen in air is the least expensive oxidant or source of oxygen atoms, a detailed understanding of metal$-O_2$ reactions is important in synthetic or industrial applications.

Our interests have focused on copper−dioxygen reactivity,[1,9,12] stimulated in large part by the occurrence of copper proteins and enzymes such as hemocyanin (an O_2 carrier in mollusks and arthropods),[6,7,13,14] and enzymes that "activate" O_2, promoting oxygen atom incorporation into biological substrates. The latter include tyrosinase,[6,7] dopamine β-monooxygenase (DBM),[15−17] and the related peptidyl α-hydroxylating monooxygenase (PHM),[18,19] as well as a bacterial membrane protein methane monooxygenase.[20] The "blue" multicopper oxidases promote substrate (e.g., amine, phenol) one-electron oxidations while reducing O_2 to water.[21,22] Amine oxidases[23,24] and galactose oxidase[25,26] effect amine → aldehyde oxidative deaminations and alcohol → aldehyde oxidative dehydrogenations, respectively. Respiratory enzymes that transduce energy via coupled proton pumping include the terminal cytochrome *c* and quinol oxidases.[27,28]

Interaction of O_2 with active site copper(I) plays a central role in these proteins. This reaction is reversible in the case of hemocyanins, and the adduct formed is a (μ-η^2:η^2-peroxo)-dicopper(II) species.[13,14] The situation is less clear for other enzymes, but initially formed Cu_n-O_2 (n = 1 or 2) adducts may undergo further transformation(s), for example, activation (by protonation and/or O−O bond cleavage) in monooxygenases[6,15] or reduction and protonation in oxidases.[21,27]

One goal in bioinorganic copper chemistry is to elucidate basic patterns of Cu_n-O_2 binding, structure, associated spectroscopy, and reactivity, in varied copper−ligand environments. Our program and others[7−9,29−36] involve a model compound approach.[1] Work since 1984 has led to the characterization of a variety of well-defined copper−dioxygen coordination complexes with varying Cu/O_2 stoichiometries (1:1 and 2:1) and different structures,[7,9,12,29,30,37] physical properties, and spectroscopy. Even transient Cu_n-O_2 species can be well characterized by employment of suitable polydentate ligands, low-temperature generation and physicochemical examination, and stopped-flow kinetic investigations.[38−43] Biomimetic investigations have led to the crystallographic characterization of four copper−dioxygen adducts, two recently described Cu/O_2 = 1:1 superoxo−copper(II) species (discussed later)[29,30] and two Cu/O_2 = 2:1 (peroxo)dicopper(II) compounds. That due to Kitajima and co-workers[7,44] is $\{Cu[HB(3,5\text{-}i\text{-}Pr_2pz)_3]\}_2(O_2)$ [$HB(3,5\text{-}i\text{-}Pr_2pz)_3$ = hydrotris(3,5-diisopropylpyrazolyl)borate anion], which has a side-on ligated (μ-η^2:η^2-peroxo)dicopper-(II) structure, with physical properties [i.e., Cu···Cu ~ 3.6 Å, ν_{O-O} ~ 750 cm^{-1} (resonance Raman), λ_{max} = ~350 nm (ϵ ~ 20 000 M^{-1} cm^{-1})], that closely match those of *Limulus polyphemus* oxyhemocyanin.[13,14]

Previously, we had generated and characterized $[\{(TMPA)Cu\}_2(O_2)]^{2+}$ (**1c**, Scheme 1), formed from the reversible reaction of O_2 with $[(TMPA)Cu(RCN)]^+$ (**1a**); this system utilizes the tripodal tetradentate ligand TMPA (Chart 1), and **1c** possesses a *trans*-μ-1,2-$Cu_2O_2^{2+}$ moiety with Cu···Cu = 4.36 Å.[45,46] The structural and physical properties of **1c** differ from those seen in $\{Cu[HB(3,5\text{-}i\text{-}Pr_2pz)_3]\}_2(O_2)$, with ν_{O-O} = 831 cm^{-1} (resonance Raman)[47] and UV−vis bands at 440 nm (ϵ = 2000 M^{-1}

(6) Fox, S.; Karlin, K. D. In *Active Oxygen in Biochemistry*; Valentine, J. S., Foote, C. S., Greenberg, A., Liebman, J. F., Eds.; Blackie Academic & Professional, Chapman & Hall: Glasgow, 1995; pp 188−231.
(7) Kitajima, N.; Moro-oka, Y. *Chem. Rev.* **1994**, *94*, 737−757.
(8) *Bioinorganic Chemistry of Copper*; Karlin, K. D., Tyeklár, Z., Eds.; Chapman & Hall: New York, 1993.
(9) Karlin, K. D., Tyeklár, Z.; Zuberbühler, A. D. In *Bioinorganic Catalysis*; Reedijk, J., Ed.; Marcel Dekker, Inc.: New York, 1993; pp 261−315.
(10) Solomon, E. I.; Tuczek, F.; Root, D. E.; Brown, C. A. *Chem. Rev.* **1994**, *94*, 827−856.
(11) Solomon, E. I.; Lowery, M. D. *Science* **1993**, *259*, 1575−1581.
(12) Karlin, K. D.; Tyeklár, Z. In *Adv. Inorg. Biochem.*; Eichhorn, G. L., Marzilli, L. G., Eds.; Prentice Hall: Englewood Cliffs, NJ, 1994; Vol. 9; pp 123−172.
(13) Magnus, K. A.; Ton-That, H.; Carpenter, J. E. *Chem. Rev.* **1994**, *94*, 727−735.
(14) Magnus, K. A.; Hazes, B.; Ton-That, H.; Bonaventura, C.; Bonaventura, J.; Hol, W. G. J. *Proteins: Struct., Funct., Genet.* **1994**, *19*, 302−309.
(15) Tian, G.; Berry, J. A.; Klinman, J. P. *Biochemistry* **1994**, *33*, 226−234.
(16) Reedy, B. J.; Blackburn, N. J. *J. Am. Chem. Soc.* **1994**, *116*, 1924−1931.
(17) Stewart, L. C.; Klinman, J. P. *Annu. Rev. Biochem.* **1988**, *57*, 551−592.
(18) Eipper, B. A.; Quon, A. S. W.; Mains, R. E.; Boswell, J. S.; Blackburn, N. J. *Biochemistry* **1995**, *35*, 2857−2865.
(19) Eipper, B. A.; Milgram, S. L.; Husten, E. J.; Yun, H.-Y.; Mains, R. W. *Protein Sci.* **1993**, *2*, 489−497.
(20) Nguyen, H. T.; Shiemke, A. K.; Jacobs, S. J.; Hales, B. J.; Lidstrom, M. E.; Chan, S. I. *J. Biol. Chem.* **1994**, *269*, 14995−15005.
(21) Solomon, E. I.; Baldwin, M. J.; Lowery, M. D. *Chem. Rev.* **1992**, *92*, 521−542.
(22) Messerschmidt, A. *Adv. Inorg. Chem.* **1993**, *40*, 121−185.
(23) Cai, D.; Klinman, J. P. *J. Biol. Chem.* **1994**, *269*, 32039−32042.
(24) Dooley, D. M.; Brown, D. E.; Clague, A. W.; Kemsley, J. N.; McCahon, C. D.; McGuirl, M. A.; Turowski, P. N.; McIntire, W. S.; Farrar, J. A.; Thomson, A. J. In *Bioinorganic Chemistry of Copper*; Karlin, K. D., Tyeklár, Z., Eds.; Chapman & Hall: New York, 1993; pp 459−470.
(25) Clark, K.; Penner-Hahn, J. E.; Whittaker, M.; Whittaker, J. W. *Biochemistry* **1994**, *33*, 12553−12557.
(26) Ito, N.; Phillips, S. E. V.; Stevens, C.; Ogel, Z. B.; McPherson, M. J.; Keen, J. N.; Yadav, K. D. S.; Knowles, P. F. *Nature* **1991**, *350*, 87−90.
(27) Iwata, S.; Ostermeier, C.; Ludwig, B.; Michel, H. *Nature* **1995**, *376*, 660−669.
(28) Tsukihara, T.; Aoyama, H.; Yamashita, E.; Tomizaki, T.; Yamaguchi, H.; Shinzawa-Itoh, K.; Nakashima, R.; Yaono, R.; Yoshikawa, S. *Science* **1995**, *269*, 1069−1074.
(29) Fujusawa, K.; Tanaka, M.; Moro-oka, Y.; Kitajima, N. *J. Am. Chem. Soc.* **1994**, *116*, 12079−12080.
(30) Harata, M.; Jitsukawa, K.; Masuda, H.; Einaga, H. *J. Am. Chem. Soc.* **1994**, *116*, 10817−10818.
(31) Lynch, W. E.; Kurtz, D. M., Jr.; Wang, S.; Scott, R. A. *J. Am. Chem. Soc.* **1994**, *116*, 11030−11038.
(32) Sorrell, T. N.; Allen, W. E.; White, P. S. *Inorg. Chem.* **1995**, *34*, 952−960.
(33) Mahapatra, S.; Halfen, J. A.; Wilkinson, E. C.; Que, L., Jr.; Tolman, W. B. *J. Am. Chem. Soc.* **1994**, *116*, 9785−9786.
(34) Uozumi, K.; Hayashi, Y.; Suzuki, M.; Uehara, A. *Chem. Lett.* **1993**, 963−966.
(35) Asato, E.; Hashimoto, S.; Matsumoto, N.; Kida, S. *J. Chem. Soc., Dalton Trans.* **1990**, 1741−1746.
(36) Caulton, K. G.; Davies, G.; Holt, E. M. *Polyhedron* **1990**, *9*, 2319−2351.
(37) Sorrell, T. N. *Tetrahedron* **1989**, *45*, 3−68.
(38) Cruse, R. W.; Kaderli, S.; Karlin, K. D.; Zuberbühler, A. D. *J. Am. Chem. Soc.* **1988**, *110*, 6882−6883.
(39) Karlin, K. D.; Wei, N.; Jung, B.; Kaderli, S.; Zuberbühler, A. D. *J. Am. Chem. Soc.* **1991**, *113*, 5868−5870.
(40) Karlin, K. D.; Wei, N.; Jung, B.; Kaderli, S.; Niklaus, P.; Zuberbühler, A. D. *J. Am. Chem. Soc.* **1993**, *115*, 9506−9514 and references cited therein.
(41) Karlin, K. D.; Nasir, M. S.; Cohen, B. I.; Cruse, R. W.; Kaderli, S.; Zuberbühler, A. D. *J. Am. Chem. Soc.* **1994**, *116*, 1324−1336.
(42) Wei, N.; Lee, D.-H.; Murthy, N. N.; Tyeklár, Z.; Karlin, K. D.; Kaderli, S.; Jung, B.; Zuberbühler, A. D. *Inorg. Chem.* **1994**, *33*, 4625−4626.
(43) Becker, M.; Schindler, S.; van Eldik, R. *Inorg. Chem.* **1994**, *33*, 5370−5371.
(44) Kitajima, N.; Fujisawa, K.; Fujimoto, C.; Moro-oka, Y.; Hashimoto, S.; Kitagawa, T.; Toriumi, K.; Tasumi, K.; Nakamura, A. *J. Am. Chem. Soc.* **1992**, *114*, 1277−1291.
(45) Tyeklár, Z.; Jacobson, R. R.; Wei, N.; Murthy, N. N.; Zubieta, J.; Karlin, K. D. *J. Am. Chem. Soc.* **1993**, *115*, 2677−2689.
(46) Jacobson, R. R.; Tyeklár, Z.; Karlin, K. D.; Liu, S.; Zubieta, J. *J. Am. Chem. Soc.* **1988**, *110*, 3690−3692.
(47) Baldwin, M. J.; Ross, P. K.; Pate, J. E.; Tyeklár, Z.; Karlin, K. D.; Solomon, E. I. *J. Am. Chem. Soc.* **1991**, *113*, 8671−8679.

Scheme 1

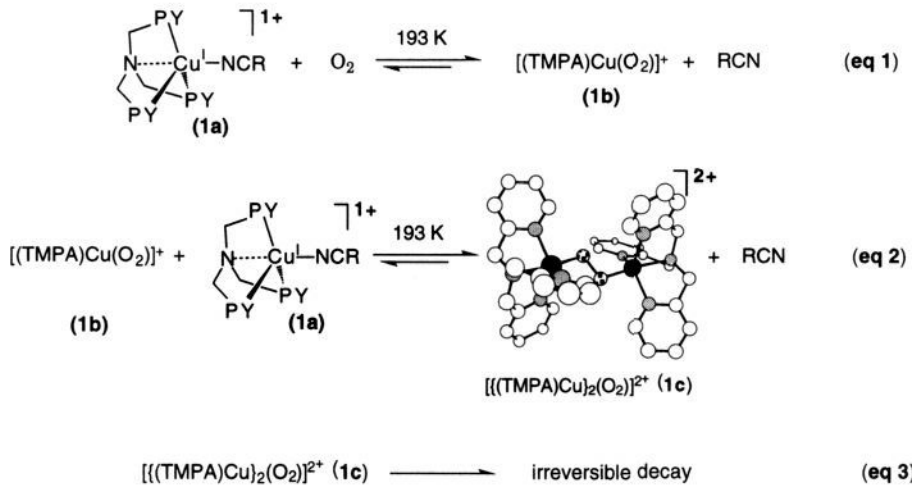

Chart 1

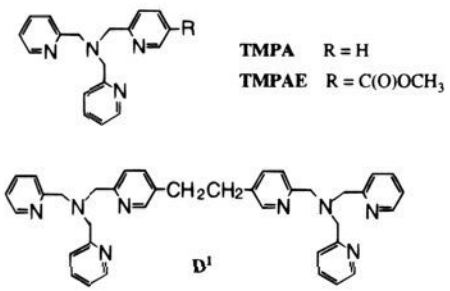

cm^{-1}), λ_{max} = 525 nm (11 500), ~600 nm (sh, ~7600), and a d–d band at 1035 nm (180). Strong, multiple absorptions in the near UV and visible spectral region can be assigned as peroxo-to-copper(II) ligand-to-metal charge-transfer (LMCT) bands.[10]

We also have reported a complete kinetics/thermodynamics investigation of the reaction of $[(TMPA)Cu(RCN)]^+$ (**1a**) (R = Me or Et)[48] with O_2.[39,40] Initially, a spectroscopically detectable (λ_{max} = 410 nm, ϵ = 4000 M^{-1} cm^{-1}) Cu/O_2 = 1:1 adduct $[(TMPA)Cu(O_2)]^+$ (**1b**) [formally a superoxo–copper(II) species] is formed; this reacts rapidly with excess **1a** to give $[\{(TMPA)Cu\}_2(O_2)]^{2+}$ (**1c**) (Scheme 1). While **1b** and **1c** can be studied at low temperatures, the room temperature stability of these (and other Cu_2O_2 complexes)[9] is rather low because of highly unfavorable reaction entropies; e.g., for **1c**, $\Delta S_{12}^\circ = -220 \pm 11$ J K^{-1} mol^{-1}.[40] We also have seen that the relative stability of Cu–O_2 1:1 species versus Cu_2–O_2 (i.e., peroxo-bridged) 2:1 complexes greatly depends on the ligand environment and imposed metal coordination, such as when pyridyl groups in TMPA are replaced by quinolyl[40,49] or imidazolyl[50] donors.

To better understand critical factors determining copper–dioxygen complex structure and O_2-binding kinetic and thermodynamic characteristics, we sought to elaborate the chemistry of the TMPA ligand system. A dinucleating analogue of TMPA, with two tripodal units joined by some organic linker group, was anticipated to stabilize peroxo copper(II) by providing an *intramolecular* version of the second step in Scheme 1. The detailed effects on kinetics/thermodynamics parameters of O_2 reaction with such a dicopper(I) complex would be of interest. Would the same type of Cu/O_2 1:1 adduct form? Would *intramolecular* binding of O_2 be considerably faster? Would the enthalpy of copper–dioxygen binding be affected? Would or could *intermolecular* chemistry occur?

Thus, the focus of this report is the chemistry of a new dinucleating ligand D^1 (Chart 1). Its synthesis and that of a new dicopper(I) complex $[(D^1)Cu^I_2(RCN)_2]^{2+}$ (**2a**) are given, the X-ray structure of **2a** is described, and its $Cu(I)_2/O_2$ chemistry is detailed. The ligand D^1 was chosen for its ease of synthesis and because hand-held models indicate that it might provide a largely unstrained environment for a peroxo–dicopper(II) structure close to that observed in $[\{(TMPA)Cu\}_2(O_2)]^{2+}$ (**1c**). We also report the $Cu(I)/O_2$ kinetics and thermodynamics of the mononuclear Cu(I) complex of TMPAE, $[(TMPAE)Cu(MeCN)]^+$ (**1a′**) (Chart 1). The X-ray analysis of **1a′** [42] has previously given insight into the distorted pentacoordinate structure of this complex and thus, by analogy, of **1a** (Scheme 1). The reactions with $[(TMPAE)Cu(MeCN)]^+$ (**1a′**) and $[(D^1)Cu^I_2(MeCN)_2]^{2+}$ (**2a**) provide additional data for $Cu(I)/O_2$ reactivity in this tripodal tetradentate ligand environment, while also giving insight into the relationship between kinetics/thermodynamics and the redox potential of the copper complex as affected by the pyridine substituent, i.e., 5-[–C(O)-OCH_3] or 5-(–CH_2CH_2)–, respectively.

Experimental Section

Methods and Reagents. Reagents and solvents were of commercially available reagent quality unless otherwise stated. Dioxygen was dried over a short column of supported P_4O_{10} (Aquasorb, Mallinkrodt). Propionitrile was first distilled over P_4O_{10}, then refluxed, and distilled from CaH_2 under argon. Diethyl ether was dried by passing it through a 50-cm column of activated alumina or by direct distillation from sodium benzophenone under Ar. In the dark, CH_2Cl_2 was stirred with concentrated sulfuric acid for several days. After being washed with water and then Na_2CO_3 solution (saturated), it was dried over anhydrous $MgSO_4$ before a final reflux and distillation from CaH_2. All ligands were made in the air unless otherwise stated. Column chromatography was carried out with alumina; the column size was typically 30 cm × 3 cm. Preparation and handling of air-sensitive materials were carried out under argon with standard Schlenk techniques. Solvents and solutions were deoxygenated by either repeated vacuum/purge cycles using argon or bubbling of argon (20 min) directly through the solution. Copper(I) solid samples were stored and transferred, and samples for NMR and IR spectra were prepared, in a Vacuum/Atmospheres drybox filled with argon. Elemental analyses were performed by Desert Analytics, Tucson, AZ.

(48) RCN, MeCN, and EtCN are used somewhat indiscriminately in formulas in this text, since compounds were normally synthesized with MeCN as an additional ligand, but all kinetics experiments were carried out in EtCN.

(49) Wei, N.; Murthy, N. N.; Chen, Q.; Zubieta, J.; Karlin, K. D. *Inorg. Chem.* **1994**, *33*, 1953–1965.

(50) Wei, N.; Murthy, N. N.; Tyeklár, Z.; Karlin, K. D. *Inorg. Chem.* **1994**, *33*, 1177–1183.

Infrared spectra were recorded neat or in Nujol mulls on a Mattson Galaxy 4030 FT-IR spectrometer. NMR spectra were measured in $CDCl_3$ or CD_3CN on either a Varian (400-MHz) or a Bruker (300-MHz) NMR instrument. All spectra were recorded in 5-mm-o.d. NMR tubes. Chemical shifts were reported as δ values downfield from internal standard Me_4Si. Low-temperature UV−vis spectral studies were carried out with a Hewlett-Packard 8452A diode array spectrometer driven by a Compaq Desk pro 386S computer and software written by OLIS, Inc. The spectrometer was equipped with a variable-temperature dewar and a cuvette assembly as described elsewhere.[51,52] Gas chromatography was carried out on a Hewlett-Packard 5890 instrument fitted with a 30-m HP-5 (cross-linked 5% phenyl methyl silicone) capillary column. Electron ionization mass spectra were obtained on a double-focusing Vacuum Generator 70-S (VG 70-S) gas chromatography/mass spectrometer. Fast atomic bombardment (FAB) mass spectra were obtained with the VG 70-S instrument.

Synthesis of Ligands: Methyl 6-(Bromomethyl)nicotinate and TMPAE. These compounds were synthesized as previously described.[45]

TMPAOH. Into a two-neck round-bottom flask was added $LiAlH_4$ (0.6 g, 15.8 mmol) under Ar, followed by 50 mL of Et_2O. At 273 K, TMPAE (5 g, 14.3 mmol) in 150 mL of distilled Et_2O was added dropwise to the $LiAlH_4$ suspension with stirring. The gray suspension of $LiAlH_4$ gradually turned yellow. The mixture was slowly warmed to room temperature and stirred overnight (18 h). The yellow suspension changed to brown with time. After the reaction was stopped, 0.6 mL of H_2O was added slowly, followed by 0.6 mL of 10% NaOH and another 0.6 mL of H_2O. When the brown suspension reacted with water, it changed to off-white and the ether layer became yellow. The precipitate was filtered off on a medium frit and washed thoroughly with diethyl ether. The ether layer was collected, combined with the previous filtrate, and dried over $MgSO_4$. The supernatant was separated and concentrated in vacuo to give a brown oil (3.8 g, 83%). This was used without further purification. ^1H NMR (CD_3CN): δ 3.75 (s, 6 H, 3 CH_2), 4.55 (s, 2 H, CH_2OH), 7.145−7.153 (m, 2 H), 7.55−7.61 (m 6 H), 8.42−8.44 (m, 3 H). IR (neat, cm^{-1}): 3250 (vs, br, OH), 2925−2850 (m, CH), 1591 (vs, C=C). Mass spectrum: *m/z* 321 $(M + 1)^+$.

TMPACl. TMPAOH (1.5 g, 4.70 mmol) in 30 mL of $CHCl_3$ was added with stirring to 10 mL of $CHCl_3$ containing 2 mL of $SOCl_2$ at 273 K. The clear yellow TMPAOH solution quickly became cloudy, and some dark oil formed. The reaction mixture was stirred overnight at room temperature. After the reaction was stopped, the solution was concentrated to dryness in vacuo to give a greenish solid. To this was added 50 mL of THF and a 5−10-fold excess of Et_3N, and the mixture was stirred for several hours, resulting in a brown solution with dark brown precipitate. After filtering through a medium frit, the filtrate was collected and concentrated in vacuo to give 2 g of brown oil, which was chromatographed on alumina, eluting with ethyl acetate. The product fraction was collected and concentrated under reduced pressure to afford a white solid (0.8 g, yield 50%) (R_f = 0.34, alumina, ethyl acetate). ^1H NMR ($CDCl_3$): δ 3.87 (s, 4 H, 2 CH_2), 3.89 (s, 2 H, CH_2), 4.57 (s, 2 H, CH_2Cl), 7.13−7.17 (m, 2 H), 7.55−7.69 (m, 6 H), 8.53−8.55 (m, 3 H). IR (Nujol, cm^{-1}): 1589 (vs, C=C), 1566 (s). Mass spectrum: *m/z* 339 $(M + 1)^+$.

Ligand D^1. Under argon, $[Cu(MeCN)_4]PF_6$ (0.8 g, 2.15 mmol) and TMPACl (0.3 g, 0.88 mmol) were added into a 100-mL Schlenk flask. Degassed MeCN (25 mL) was added to the white solid mixture. The solids initially turned to yellow and quickly changed to green; the solution mixture was stirred under argon overnight. The MeCN solvent was evaporated under reduced pressure, giving a green-blue solid. Dichloromethane (50 mL) was added to the solid, and aqueous ammonia (50 mL) was added to strip out the organic ligand. The CH_2Cl_2 layer was collected, the ammonia extraction was repeated, and then the organic layer was washed with water three times. The organic layer was collected and concentrated in vacuo to give a brown oil, which was column chromatographed and eluted with ethyl acetate. The product fraction was collected and the ethyl acetate removed under reduced pressure to afford an off-white solid (50% yield) (R_f = 0.11, alumina, ethyl acetate). ^1H NMR ($CDCl_3$): δ 2.89 (s, 4 H, CH_2CH_2), 3.86 (s, 4 H, 2 CH_2), 3.89 (s, 8 H, 4 CH_2), 7.16−7.12 (m, 4 H), 7.57−7.6 (m, 12 H), 8.35 (d, 2 H), 8.54 (d, 4 H). IR (neat, cm^{-1}): 3061−2926 (m, CH), 1591 (vs, C=C), 1570 (s), 1476 (m), 1433 (s), 1366 (m), 1123 (m). Mass spectrum: *m/z* 606 (M^+). FAB mass spectrum: *m/z* 607 $(M + 1)^+$.

Synthesis of Cu(I) Complexes: [(TMPAE)Cu(MeCN)](PF_6) (1a'-PF_6). This was synthesized according to the published procedure.[45]

$[(D^1)Cu_2(MeCN)_2](ClO_4)_2$ [2a-$(ClO_4)_2$]. Dioxygen-free MeCN (10 mL) was added to solids D^1 (0.108 g, 0.165 mmol) and $[Cu(MeCN)_4]$-ClO_4 (0.0977 g, 0.299 mmol) in a 100-mL Schlenk flask under argon. Dry diethyl ether (ca. 20 mL) was added to the yellow solution until a slight cloudiness was observed. The solution mixture was filtered through a medium frit. An additional portion of diethyl ether was added to completely precipitate the yellow solid. The supernatant was decanted, and the solid was washed with ether. Drying the yellow solid under vacuum for 2.5 h yielded 0.11 g (73%) of yellow microcrystalline material. Anal. Calcd for $Cu_2C_{42}H_{44}N_{10}Cl_2O_8$: C, 49.66; H, 4.33; N, 13.79. Found: C, 49.79; H, 4.38; N, 13.66. ^1H NMR (CD_3CN, room temperature): δ 1.97 (s, 6H, 2 MeCN), 2.92 (s, 4 H, CH_2CH_2), 3.5−4.5 (br), 7.5−9 (br). ^1H NMR (CD_3CN, 230 K): δ 1.97 (s, 6 H, 2 MeCN), 2.92 (s, 4 H, CH_2CH_2), 3.84 (s, 12 H, 6 CH_2), 7.32−8.59 (m, 22 H). IR (Nujol, cm^{-1}): 2010 (m, ClO_4^- overtone), 1599 (s, C=C), 1084 (vs, ClO_4^-). X-ray quality yellow crystals were obtained by dissolving 0.1 g of dicopper(I) complex in 5−8 mL of oxygen-free propionitrile and then carefully layering the solution with diethyl ether; crystals of $[(D^1)Cu_2(EtCN)_2](ClO_4)_2$ developed in 2−3 days.

Dioxygen Uptake Manometry. O_2 absorption by **2a**-$(ClO_4)_2$ at 193 K was monitored at constant pressure in a glass buret as previously described.[51,52] A 25-mL side-arm Schlenk flask containing a propionitrile solution of $[(D^1)Cu_2(MeCN)_2](ClO_4)_2$ (0.457 g, 0.45 mmol) was attached to the manometer system and cooled to 193 K under argon. After evacuation of the flask for 1 h, the stopcock leading to the reaction flask was closed and the buret assembly was equilibrated to 1 atm of O_2 pressure. Then, O_2 was allowed to enter the reaction flask, causing the solution to immediately change to deep purple as the Cu(I) complex reacted. The volume of O_2 taken up was 9.4 mL (after accounting for solvent O_2 uptake), corresponding to a Cu(I)/O_2 ratio of 2.14(±0.05): 1.

Quantitative Determination of O_2 Liberation from $[(D^1)Cu_2(O_2)]^{2+}$ (2c) and Synthesis of $[(D^1)Cu_2(PPh_3)_2](ClO_4)_2$. After the manometric reaction with O_2 was completed, under a dioxygen flow a storage tube containing triphenylphosphine (0.3 g, 1.1 mmol) and filled with O_2 was attached to the Schlenk flask. After the system was equilibrated for 1 h at 193 K, the triphenylphosphine was added to the reaction flask. During 4 h, 7.2 mL of oxygen was liberated from the reaction [76% recovery of the dioxygen originally taken up by dicopper(I) complex], with formation of a light green solution. The propionitrile solvent was removed by application of a vacuum, giving a light green residue. This green mixture was recrystallized from acetonitrile/ether, resulting in a pale yellow powder of $[(D^1)Cu_2(PPh_3)_2](ClO_4)_2$ (0.47 g, 73% yield). Elemental anal. of $[(D^1)Cu_2(PPh_3)_2](ClO_4)_2$. Calcd for $Cu_2C_{74}H_{68}N_8P_2Cl_2O_8$: C, 60.92; H, 4.67; N, 7.68. Found: C, 60.75; H, 4.44; N, 7.30. ^1H NMR (CD_3CN): δ 2.51 (s, 4 H, CH_2CH_2), 3.98 (s, 4 H, 2 CH_2), 4.04 (s, 8 H, 4 CH_2), 7.17−7.44 (m, 42 H), 7.68−7.70 (m, 4 H), 7.90 (s, 2 H), 8.25 (s, 4 H).

Electrochemistry. Cyclic voltammetry and bulk electrolysis were carried out with a Bioanalytical Systems BAS-100B electrochemistry analyzer connected to a HP-7440A plotter. The cell was a modified standard three-chambered design for handling air-sensitive solutions by use of high-vacuum valves with Viton O-ring seals. Either a platinum disk (BAS MF 2013) or a glassy carbon electrode (GCE, BAS MF 2012) was used as the working electrode. The reference electrode was $Ag^+/AgNO_3$. The measurements were performed at room temperature in DMF solvent containing 0.2 M tetrabutylammonium hexafluorophosphate (TBAHP) and 10^{-3}−10^{-4} M copper complex deoxygenated by bubbling it thoroughly with argon.

Stopped-Flow Kinetics Studies. These rapid O_2-binding reactions were followed with a diode-array (359−776 nm, 508 diodes) stopped-flow instrument over the temperature range 180−296 K in dry

(51) Karlin, K. D.; Cruse, R. W.; Gultneh, Y.; Farooq, A.; Hayes, J. C.; Zubieta, J. *J. Am. Chem. Soc.* **1987**, *109*, 2668−2679.

(52) Karlin, K. D.; Haka, M. S.; Cruse, R. W.; Meyer, G. J.; Farooq, A.; Gultneh, Y.; Hayes, J. C.; Zubieta, J. *J. Am. Chem. Soc.* **1988**, *110*, 1196−1207.

Scheme 2

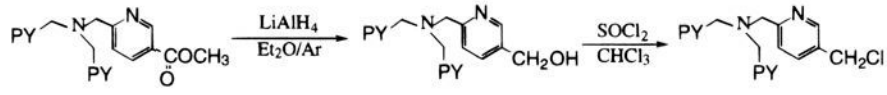

TMPAE **TMPAOH** **TMPACl**

PY = 2-pyridyl

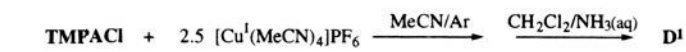

propionitrile and the data subjected to factor analysis and subsequently global analysis using the program KINFIT.[40] As all of the reaction mechanisms tested were complicated, including steps of second or even third order in concentration of the complex, numerical integration of the appropriate differential equations was used throughout. Fixed spectra of Cu(I) complex and/or dioxygen adducts were used as needed for successful analysis, prominently for separation of forward and reverse rate constants of a given equilibrium and for direct determination of thermodynamic parameters in fast equilibria. Calculation of temperature-dependent analytical concentrations and further details are given in accounts of kinetic/thermodynamic studies of copper(I)–complex O_2 reactivity.[40,41] Besides the reaction steps describing pseudoreversible dioxygen interaction, to be discussed in detail below, normally (and specifically at higher temperatures) slow, ill-defined, irreversible decay was observed. Corresponding rate constants were included into the numerical analysis when needed for fitting purposes, but not analyzed any further.

For [(TMPAE)Cu(MeCN)]$^+$ (**1a′**), a total of 64 measurements were used for the final calculations. The concentration of **1a′**-PF_6 was 5.55 $\times$ 10^{-4} M and $[O_2]$ = 4.4 $\times$ 10^{-3} M in the mixed solution. The temperature was varied between 181 and 270 K, and the data collection time ranged from 0.6 to 24 s. Experiments with **1a′**-PF_6 = 1.19 $\times$ 10^{-3} M also were carried out to check the reproducibility of the system.

For [$(D^I)Cu^I_2(MeCN)_2$]$^{2+}$ (**2a**), eight different Cu(I) concentrations were used to carry out a total of 324 measurements for the final calculations (all series reacted with oxygen-saturated propionitrile solution, $[O_2] = 8.8 \times 10^{-3}$ M).[40] The concentrations of mixed Cu(I) solutions were (0.652–6.97) $\times$ 10^{-4} M. The temperature was varied between 180 and 296 K, and the data collection time ranged from 0.5 to 60 s.

Results and Discussion

Ligand Synthesis. The novel dinucleating ligand D^I was made through a multistep process summarized in Scheme 2 (also see Experimental Section), in fact proceeding via the previously synthesized intermediate TMPAE.[45] The final step of the synthesis of D^I used copper(I) as the coordinating ion and reductant for the reductive coupling reaction of the activated halide TMPACl. Low-oxidation-state transition metals effect similar processes involving organic halides; we previously have shown that [(TMPA)Cu^I(RCN)]$^+$ (**1a**) can be used to reductively couple a variety of benzylic or other activated organic halides.[53] Here, we found that addition of [$Cu^I(MeCN)_4$]$^+$ to TMPACl, containing the tetradentate TMPA moiety, provided coupled product D^I, isolatable in ~50% yield.

Copper(I) Complex Syntheses. [(TMPAE)Cu(MeCN)](PF_6) (**1a′**-PF_6) was synthesized as previously described.[45] The dicopper(I) complex with D^I, [$(D^I)Cu_2(MeCN)_2$]$^{2+}$ (**2a**), was generated by adding 1 equiv of the dinucleating ligand to 2 equiv of [$Cu(MeCN)_4$](ClO_4) under Ar, as described previously for **1a′**.[45] The synthesis and handling/study of the Cu(I)

$$2[Cu(MeCN)_4](ClO_4) + D^I \rightarrow [(D^I)Cu_2(MeCN)_2](ClO_4)_2$$
$$\textbf{2a}\text{-}(ClO_4)_2$$

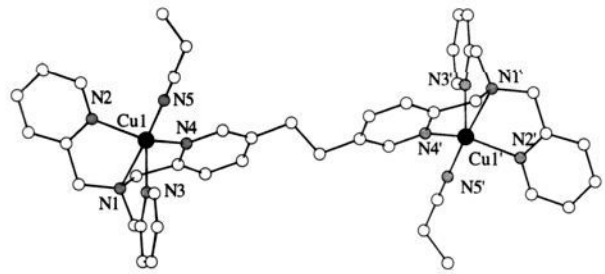

Figure 1. Chem 3-D drawing of [$(D^I)Cu_2(EtCN)_2$]$^{2+}$ (**2a**). Selected bond distances (Å) and angles (deg): Cu1–N1, 2.423(4); Cu1–N2, 2.097(4); Cu1–N3, 2.111(4); Cu1–N4, 2.071(4); Cu1–N5, 1.984(4); N5–$C51_{nitrile}$, 1.116(6); Cu1···Cu1, 11.705(2); N1–Cu1–N2, 74.9(2); N1–Cu1–N3, 74.1(2); N1–Cu1–N4, 76.0(1); N1–Cu1–N5, 176.2(1); N2–Cu1–N3, 116.7(2); N2–Cu1–N4, 109.1(1); N2–Cu1–N5, 104.5(2); N3–Cu1–N4, 114.7(1); N3–Cu1–N5, 103.2(2); N4–Cu1–N5, 107.6(2); Cu1–N5–$C51_{nitrile}$, 178.3(5).

complexes must be carried out exclusively in organonitrile solvents. In CH_2Cl_2, **1a**,[45,53] **1a′**, and **2a** all react rapidly with solvent by abstracting a chlorine atom, producing chloro–copper(II) complexes; this behavior also has been observed for copper(I) complexes with tripodal tetradentate ligands containing either quinolyl[49] or imidazolyl donors.[50] A bis-triphenylphosphine adduct complex [$(D^I)Cu(PPh_3)_2$]$^{2+}$ also was generated, by reacting 2 equiv of PPh_3 with [$(D^I)Cu_2(O_2)$]$^{2+}$ in propionitrile solvent at 193 K (vide infra).

The presence of the organonitrile ligands in [(TMPAE)Cu(MeCN)]$^+$ (**1a′**) and [$(D^I)Cu^I_2(MeCN)_2$]$^{2+}$ (**2a**) was confirmed from C, H, N analysis, NMR spectroscopy, and an X-ray crystal structure study of a propionitrile analogue, [$(D^I)Cu_2(EtCN)_2$]$^{2+}$. Nitrile coordination is observed in many other cases where related tripodal tetradentate ligands contain three pyridine rings.[45,54] By contrast, copper(I) complexes with tripodal ligands containing quinolyl[49] or imidazolyl[50] donor groups do not possess any additional coordinated nitrile ligand, at least in the isolated solids. This difference may be due to the size of the donor group (especially in the quinolyl case) and might also be related to the unexpected lack of O_2 binding to the imidazolyl compounds.

X-ray Structure of [$(D^I)Cu_2(EtCN)_2$](ClO_4)$_2$ (2a-(ClO_4)$_2$). Details of the X-ray structure determination and complete tables with positional and thermal parameters, bond distances, and bond angles have been published.[42] The structure of **2a** consists of a centrosymmetric [$(D^I)Cu_2(EtCN)_2$]$^{2+}$ dication with Cu1···Cu1′ = 11.70 Å (Figure 1). Each Cu(I) center is identically bonded to three pyridyl nitrogen atoms and a nitrogen atom from a propionitrile group. The Cu–N_{py} distances (2.07–2.11 Å) are close to those found in similar mononuclear copper(I) complexes with tripodal tetradentate ligands;[45] however, they are slightly longer than those observed in tetracoordinated copper(I) complexes (2.0–2.05 Å) with related ligands.[51,55,56]

(53) Jacobson, R. R.; Tyeklár, Z.; Karlin, K. D. *Inorg. Chim. Acta* **1991**, *181*, 111–118.

(54) Jacobson, R. R. Ph.D. Thesis, State University of New York at Albany, 1989.

The short Cu1−N_{RCN} distance, 1.98 Å, indicates that the nitrile group is strongly coordinated to the Cu(I) center, as observed in many nitrile-coordinated copper(I) complexes.[45,52] The Cu(I) ions in **2a** are pentacoordinate, but the geometry may be better described as distorted from tetrahedral, with only a weak interaction between Cu(I) and the "hard" tertiary amine nitrogen N1; Cu1−N1 = 2.423 Å, a value that lies outside the sum of the covalent radii of Cu and N. The N1 nitrogen lone pair clearly points toward the Cu1, as the N1 atom lies 0.341 Å out of the plane (toward copper) formed by the three benzylic carbon atoms. The Cu1 atom is 0.543 Å out of the N2, N3, N4 plane, toward the propionitrile N5 nitrogen atom. Relevant dihedral angles are Cu1−N3−N4/Cu−N2−N5 = 85.99°, Cu1−N3−N5/Cu1−N2−N4 = 88.08°, and Cu1−N4−N5/(Cu1−N2−N3 = 92.06°. Thus, the copper ligation found in $[(D^1)Cu_2(EtCN)_2]^{2+}$ (**2a**) is very similar to that observed for the ester-containing complex $[(TMPAE)Cu(MeCN)]^+$ (**1a′**)[45] and in most Cu(II) complexes with this tripodal tetradentate ligand, e.g., $[(TMPA)Cu^{II}Cl]^+$.[56]

^{1}H NMR Spectrum of $[(D^1)Cu_2(MeCN)_2]^{2+}$ (2a). At room temperature, the ^{1}H NMR spectrum of D^1 is sharp and the protons of all methylene and pyridine groups are nicely separated. A room-temperature spectrum of **2a** is dramatically broadened by comparison (Figure S1, supporting information). The aliphatic protons from the six CH_2 groups directly connected to the N1 and N1′ nitrogen atoms and protons of the 6-position of all pyridine rings are not detected. However, aliphatic protons of the $-CH_2CH_2-$ linker between tetradentate L groups, i.e., those further from the Cu(I) centers, are relatively sharp. While a detailed study has not been undertaken for **2a**, we have previously shown that $[(TMPA)Cu(MeCN)]^+$ (**1a**) exhibits dynamic behavior in solution,[54,57] most likely involving coordination exchange where one pyridyl arm is cleaved from the copper ion, as indicated below.

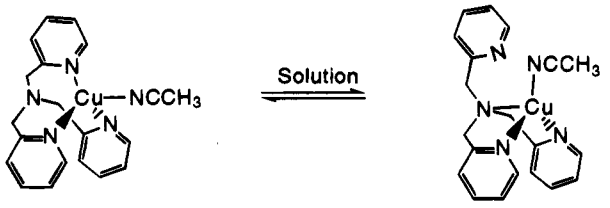

Exactly such a structure is observed in the triphenylphosphine adduct $[(TMPA)Cu^I(PPh_3)]^+$, where one pyridyl donor dangles and is uncoordinated.[45] Thus, broadening of methylene and pyridyl resonances could occur in solution, as the pyridyl groups exchange from "on" to "off" positions. This exchange should be temperature dependent, as observed.[57] In fact the ^{1}H NMR spectrum of **2a** is sharp when recorded at lower temperature; a 230 K spectrum is shown in Figure S1 (supporting information). Here, all the resonances expected for this diamagnetic dicopper(I) complex **2a** are observed.

Electrochemistry. The half-wave redox potentials for the copper(I) complexes $[(TMPA)Cu(MeCN)]^+$ (**1a**), $[(TMPAE)Cu(MeCN)]^+$ (**1a′**), and $[(D^1)Cu_2(MeCN)_2]^{2+}$ (**2a**) were measured by cyclic voltammetry (CV) under argon in dimethylformamide (DMF). The results are provided in Table 1. All copper(I) complexes displayed quasi-reversible behavior with i_{pa}/i_{pc} close to unity. Peak separations were all less than 90 mV at a scan rate of 100 mV/s. The ferrocene/ferrocenium couple under the same conditions showed ΔE_p = 89 mV and $E_{1/2}$ = 20 mV vs $Ag/AgNO_3$.

Table 1. Cyclic Voltammetry Data for Copper(I) Complexes in DMF

complexes	$E_{1/2}$ (mV)[a]	ΔE_p (mV)	i_{pa}/i_{pc}
$[(TMPA)Cu(MeCN)]^+$ (**1a**)	−608	78	0.80
$[(TMPAE)Cu(MeCN)]^+$ (**1a′**)	−550	88	0.85
$[(D^1)Cu_2(MeCN)_2]^{2+}$ (**2a**)	−619	88	1.00
$[(BQPA)Cu]^+$ [b]	−410[b]	95	0.96

[a] Versus $Ag/AgNO_3$. [b] Reference 49.

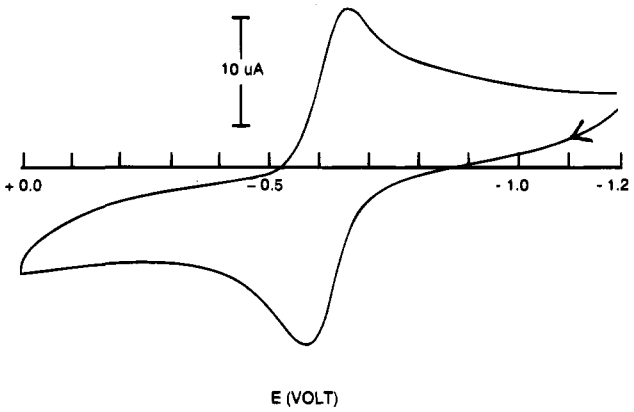

Figure 2. Cyclic voltammogram of $[(D^1)Cu^I_2(MeCN)_2]^{2+}$ (**2a**) in DMF. Scan rate = 100 mV/s.

A typical CV scan for $[(D^1)Cu^I_2(MeCN)_2]^{2+}$ (**2a**) is given in Figure 2. Results from bulk electrolysis correspond to a two-electron process per dicopper complex, corroborated by comparison with the behavior of mononuclear **1a**. These experiments were accompanied by a color change from yellow [i.e., Cu(I) complex] to blue-green [i.e., oxidized Cu(II) species]. The CV of a coulometrically oxidized solution gave the exact complement to that of the original Cu(I) complex solution at the same scan rate. These observations demonstrate an effective reversibility via an overall two-electron-transfer reaction:

$$[(D^I)Cu^{II}_2]^{4+} + 2e^- \rightleftharpoons [(D^I)Cu^I_2]^{2+}$$
2a

The electrochemical behavior of $[(D^1)Cu^I_2(MeCN)_2]^{2+}$ (**2a**) is best explained with a pair of non-interacting copper(I) centers, as also implied by the solid-state structure. The presence of only one apparent redox CV wave has been well-documented in a number of other dicopper(I) and/or dicopper(II) complexes lacking a tight bridging ligand (e.g., halide, RO^-, etc.), derived from dinucleating ligands with some flexible organic linker between chelating moieties.[58−61] If $\Delta E_{1/2}$ between two separate processes (i.e., $Cu^{II}-Cu^{II} + e^- \rightarrow Cu^{II}-Cu^I + e^- \rightarrow Cu^I-Cu^I$) is $<\sim$100−200 mV, only one wave is generally seen. We have not attempted a more detailed analysis which could be used to estimate the $E_{1/2}$ for the individual redox reactions,[62] but this has been carried out in a number of cases.[60,61]

The $E_{1/2}$ value (Table 1) for $[(D^1)Cu^I_2(MeCN)_2]^{2+}$ (**2a**) is very close to that of the "parent" mononuclear complex $[(TMPA)Cu(MeCN)]^+$ (**1a**). Many factors are known to influence the

(55) Karlin, K. D.; Hayes, J. C.; Hutchinson, J. P.; Hyde, J. R.; Zubieta, J. *Inorg. Chim. Acta* **1982**, *64*, L219−L220.
(56) Karlin, K. D.; Hayes, J. C.; Shi, J.; Hutchinson, J. P.; Zubieta, J. *Inorg. Chem.* **1982**, *21*, 4106−4108.
(57) Crans, D. C.; Karlin, K. D. Unpublished NMR spectroscopic observations.
(58) Karlin, K. D.; Tyeklár, Z.; Farooq, A.; Haka, M. S.; Ghosh, P.; Cruse, R. W.; Gultneh, Y.; Hayes, J. C.; Toscano, P. J.; Zubieta, J. *Inorg. Chem.* **1992**, *31*, 1436−1451.
(59) Mazurek, W.; Bond, A. M.; O'Connor, M. J.; Wedd, A. G. *Inorg. Chem.* **1986**, *25*, 906−915.
(60) Ciampolini, M.; Fabbrizzi, L.; Perotti, A.; Poggi, A.; Seghi, B.; Zanobini, F. *Inorg. Chem.* **1987**, *26*, 3527−3533.
(61) Oshio, H. *J. Chem. Soc., Dalton Trans.* **1990**, 2985−2989.
(62) Richardson, D. E.; Taube, H. *Inorg. Chem.* **1981**, *20*, 1278.

Table 2. UV−Vis Spectral Data for Copper(I) and Copper Dioxygen Complexes in EtCN: λ_{max}/nm (ϵ/M^{-1} cm^{-1})[a]

[(TMPA)Cu(RCN)]$^+$ (**1a**)	[(TMPA)Cu(O_2)]$^+$ (**1b**)	[{(TMPA)Cu}$_2$(O_2)]$^{2+}$ (**1c**)
343 (5600)	410 (4000)	440 (4000) sh
		525 (11500)
	580 (1100)	590 (7600) sh
	747 (1000)	1035 (160)
[(TMPAE)Cu(RCN)]$^+$ (**1a'**)	[(TMPAE)Cu(O_2)]$^+$ (**1b'**)	[{(TMPAE)Cu}$_2$(O_2)]$^{2+}$ (**1c'**)
342 (4700)	415 (3330)	445 (2000) sh
		532 (9380)
	591 (930)	590 (7000) sh
	760 (950)	nd
[(D^1)Cu_2($MeCN)_2$]$^{2+}$ (**2a**)	[(D^1)Cu_2($O_2)_2$]$^{2+}$ (**2b'**)[b]	[(D^1)Cu_2(O_2)]$^{2+}$ (**2c**)[c]
350 (5900/Cu(I))	416 (4500)	450 (1100) sh
		540 (11100)
	583 (1060)	600 (8700) sh
	755 (1110)	1010 (190)

[a] ϵ values given per Cu_nO_2 (n = 1 or 2) moiety; nd = not determined. [b] This is the 2:2 "open" adduct, eq 8 (see below). The spectrum of the 2:1 superoxo adduct **2b** was not independently determined but was taken as the arithmetic mean of those of **2a** and **2b'**. [c] After secondary rearrangement (**2c** → **2d**, see below), we found λ_{max} = 529 nm, ϵ = 9320 M^{-1} cm^{-1}; λ_{max} = 436 nm, ϵ = 2000 M^{-1} cm^{-1}; λ_{max} = 595 nm, ϵ = 7200 M^{-1} cm^{-1}. [d] The experimental source of the molar absorptivities was either benchtop experiments or kinetic/spectroscopic analyses. Any differences observed were within the error limits.

redox potentials of copper complexes including (a) the flexibility or constraints imposed by chelating ligands, (b) the types of donor atoms, and (c) the geometry of tetracoordinate complexes.[63−67] Here, all the Cu(I) complexes possess identical ligand donor atoms, and so differences could only arise from varying substituents on pyridyl ligand donors. The differences in $E_{1/2}$ values between the three complexes in question are rather small (Table 1). The observed trends are, however, in the expected direction: (1) The moderately electron donating ethyl group of the D^1 ligand linker might be the cause of the slightly more negative redox potential observed in **2a** as compared to **1a**, while (2) the electron-withdrawing ester group in the meta position relative to the pyridyl-nitrogen donor atom may be responsible for the positive shift in $E_{1/2}$ seen in **1a'** relative to **1a**. Similar effects of electron-donating and -withdrawing substituents have been seen in bipyridyl-containing Cu−ligand complexes.[68]

Low-Temperature Reaction of O_2 with [(TMPAE)Cu(MeCN)]$^+$ (1a') and [(D^1)Cu_2($MeCN)_2$]$^{2+}$ (2a). O_2-Uptake Manometry. Experiments were performed at 193 K in propionitrile to confirm the stoichiometry of reaction of O_2 with dinuclear **2a** (Experimental Section). The results show absorption of dioxygen by [(D^1)Cu_2($MeCN)_2$]($ClO_4)_2$ [**2a**-($ClO_4)_2$] (0.457 g, 0.45 mmol) in the ratio of Cu/O_2 = 2.14(±0.05); thus, the solution complex is formulated as [(D^1)Cu_2(O_2)]($ClO_4)_2$ [**2c**-($ClO_4)_2$]. This Cu/O_2 stoichiometry is identical to that of the parent [(TMPA)Cu(RCN)]$^+$ (**1a**) complex.[45]

Reaction of [(D^1)Cu_2(O_2)]($ClO_4)_2$ (2c-($ClO_4)_2$) with PPh_3: Quantitative Measurement of the Release of O_2 and Isolation of [(D^1)Cu_2($PPh_3)_2$]($ClO_4)_2$. Triphenylphosphine is a good ligand for Cu(I) complexes and has been used to characterize the reactivity of Cu_2−O_2^{2+} species.[69] At 193 K, [(D^1)Cu_2(O_2)]($ClO_4)_2$ (0.45 mmol) reacted with PPh_3 (0.3 g, 1.1 mmol) to form a copper(I)−PPh_3 complex with concomitant liberation of a gas presumed to be O_2, by analogy to the similar reaction

Scheme 3

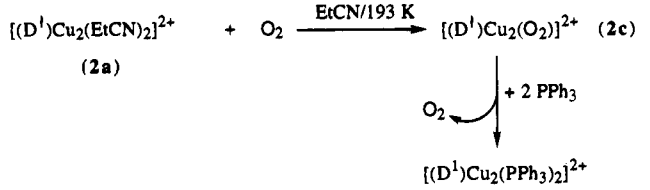

with other Cu_2O_2 complexes.[45,69] The amount of O_2 evolved was quantified by manometry (76% recovery, Experimental Section). The reaction of **2c** with PPh_3 proceeds over a 5−6-h period at 193 K. The intense purple color of peroxo−dicopper complex [(D^1)Cu_2(O_2)]$^{2+}$ (**2c**) diminished, and a light green solution formed. After removal of solvent and recrystallization from acetonitrile−ether, a pale yellow dicopper(I) complex [(D^1)Cu_2($PPh_3)_2$]($ClO_4)_2$ was obtained (73% yield) and was characterized by ^{1}H NMR spectroscopy and C, H, N analysis. The green color observed is presumed to be due to small amounts of oxidized impurities present before the mixture was fractionally recrystallized. Gas-chromatographic analysis of the collected filtrate showed only a trace amount of O=PPh_3 formed. These results suggest that [(D^1)Cu_2(O_2)]$^{2+}$ (**2c**) is a copper dioxygen complex and that the O−O bond in this species remains unbroken. Thus, the transformations observed for dinuclear **2a** in reactions with O_2 and PPh_3 are strictly analogous, Scheme 3, to the chemistry of [(TMPA)Cu(RCN)]$^+$ (**1a**).[45]

UV−Vis Spectra of O_2 Adducts. Benchtop and Stopped-Flow Determination. In bench-top experiments, reaction of [(TMPAE)Cu(MeCN)]$^+$ (**1a'**) with O_2 in EtCN at 193 K resulted in a rapid change to an intensely purple colored solution. Spectral characteristics agree closely with those observed for oxygenation of [(TMPA)Cu(MeCN)]$^+$ (**1a**)[45] (cf. Table 2), corresponding to the 2:1 (Cu/O_2) adduct [{(TMPAE)Cu}$_2$(O_2)]$^{2+}$ (**1c'**). Upon exposure to dioxygen at 193 K, a yellow propionitrile solution of the dicopper(I) [(D^1)Cu_2($MeCN)_2$]$^{2+}$ (**2a**) also rapidly converts to an intense purple color with strong and multiple UV−vis features (Figure S2, supporting information; Table 2). A weaker broad feature, ascribed to d−d transition(s), is seen at 1010 nm. The formation of the purple species [(D^1)Cu_2(O_2)]$^{2+}$ (**2c**) is completed by the time the solution of **2a** is bubbled with O_2 and inserted into the spectrometer.

Numerical analysis of diode-array stopped-flow measurements shows that the reaction of [(TMPAE)Cu(MeCN)]$^+$ (**1a'**) or

(63) Patterson, G. S.; Holm, R. H. *Bioinorg. Chem.* **1975**, *4*, 257−275.
(64) Karlin, K. D.; Gultneh, Y. *Prog. Inorg. Chem.* **1987**, *35*, 219−327.
(65) Karlin, K. D.; Sherman, S. E. *Inorg. Chim. Acta* **1982**, *65*, L39−L40.
(66) Addison, A. W. *Inorg. Chim. Acta* **1989**, *162*, 217−220.
(67) Hathaway, B. J. In *Comprehensive Coordination Chemistry*; Wilkinson, G., Ed.; Pergamon: New York, 1987; Vol. 5, pp 533−774.
(68) James, B. R.; Williams, R. J. P. *J. Chem. Soc.* **1961**, Part 2, 2007.
(69) Paul, P. P.; Tyeklár, Z.; Jacobson, R. R.; Karlin, K. D. *J. Am. Chem. Soc.* **1991**, *113*, 5322−5332.

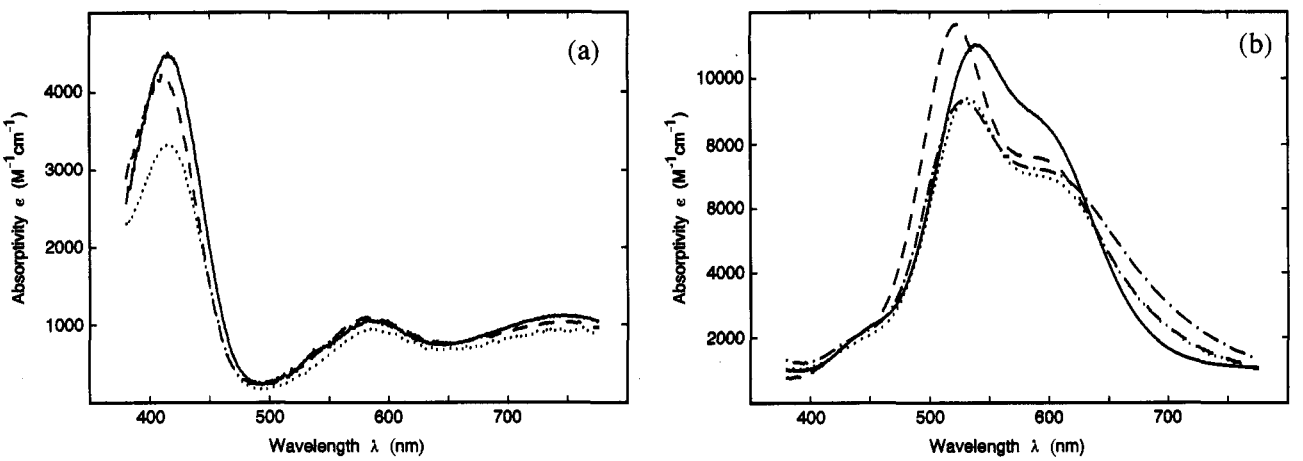

Figure 3. UV–vis spectra of (a) Cu/O_2 = 1:1 intermediates (– – –) $[(TMPA)Cu(O_2)]^+$ (**1b**), (···) $[(TMPAE)Cu(O_2)]^+$ (**1b′**), and (—) $[(D^1)Cu_2(O_2)_2]^{2+}$ (**2b′**) and (b) Cu/O_2 = 2:1 peroxo dicopper(II) species (– – –) $[\{(TMPA)Cu\}_2(O_2)]^{2+}$ (**1c**), (···) $[\{(TMPAE)Cu\}_2(O_2)]^{2+}$ (**1c′**), (—) $[(D^1)Cu_2(O_2)]^{2+}$ (**2c**), and (–·–) $[\{(D^1)Cu_2(O_2)\}_n]^{2n+}$ (**2d**) generated through numerical analysis of diode-array stopped-flow measurements.

Table 3. Kinetic Parameters for O_2 Interaction with Copper(I) Complexes **1a**, **1a′**, and **2a**[a]

		TMPA[b] (**1a**)	TMPAE (**1a′**)	D^1 (**2a**)
k_1 (M^{-1} s^{-1})	183 K	$(1.8 \pm 0.1) \times 10^4$	$(8.2 \pm 0.4) \times 10^3$	$(1.63 \pm 0.01) \times 10^4$
	223 K	$(9 \pm 4) \times 10^5$	4×10^5 [c]	$(2.0 \pm 0.3) \times 10^5$
	298 K	8×10^7	4×10^7 [c]	$(4 \pm 1) \times 10^6$
	$\Delta H_1^{\ddagger}$ (kJ mol^{-1})	32 ± 4	31 ± 5	20 ± 1
	$\Delta S_1^{\ddagger}$ (J K^{-1} mol^{-1})	14 ± 18	5 ± 29	-53 ± 6
k_{-1} (s^{-1})	183 K	8 ± 1	29 ± 2	8.0 ± 0.2
	223 K	$(3 \pm 1) \times 10^4$	6×10^4 [c]	$(6.3 \pm 0.8) \times 10^3$
	298 K	2×10^8	4×10^8 [c]	$(1.4 \pm 0.5) \times 10^7$
	$\Delta H_{-1}^{\ddagger}$ (kJ mol^{-1})	66 ± 4	63 ± 5	55 ± 1
	$\Delta S_{-1}^{\ddagger}$ (J K^{-1} mol^{-1})	137 ± 18	132 ± 29	76 ± 6
k_2 (s^{-1})	183 K	$(3.2 \pm 0.2) \times 10^1$ [d]	$(1.52 \pm 0.05) \times 10^1$ [d]	$(3.51 \pm 0.05) \times 10^1$
	223 K	$(2.48 \pm 0.02) \times 10^2$ [d]	$(2.4 \pm 0.1) \times 10^2$ [d]	$(3.3 \pm 0.1) \times 10^3$
	298 K	$(1.8 \pm 0.1) \times 10^3$ [d]	$(5.8 \pm 0.9) \times 10^3$ [d]	$(6.8 \pm 0.5) \times 10^5$
	$\Delta H_2^{\ddagger}$ (kJ mol^{-1})	14 ± 1	21 ± 1	37 ± 1
	$\Delta S_2^{\ddagger}$ (J K^{-1} mol^{-1})	-78 ± 2	-43 ± 3	-9 ± 2
k_{-2} (s^{-1}) ($=k_{off}$)	183 K	$(1.5 \pm 0.8) \times 10^{-4}$	$(2.1 \pm 0.4) \times 10^{-5}$	$(3.9 \pm 0.3) \times 10^{-1}$
	223 K	0.29 ± 0.04	$(6.4 \pm 0.4) \times 10^{-2}$	$(3.5 \pm 0.2) \times 10^1$
	298 K	$(1.2 \pm 0.3) \times 10^3$	$(7 \pm 1) \times 10^2$	$(6.7 \pm 0.9) \times 10^3$
	$\Delta H_{-2}^{\ddagger}$ (kJ mol^{-1})	61 ± 3	66 ± 1	37 ± 1
	$\Delta S_{-2}^{\ddagger}$ (J K^{-1} mol^{-1})	19 ± 10	33 ± 5	-49 ± 3
k_3 (M^{-5} s^{-1})	183 K			$(7 \pm 2) \times 10^{15}$
	223 K			$(7 \pm 1) \times 10^{14}$
	298 K			$(5.1 \pm 0.2) \times 10^{13}$
	$\Delta H_3^{\ddagger}$ (kJ mol^{-1})			-21 ± 1
	$\Delta S_3^{\ddagger}$ (J K^{-1} mol^{-1})			-54 ± 5
k_{-3} (s^{-1})	183 K			$(2.1 \pm 0.7) \times 10^{-13}$
	223 K			$(1.4 \pm 0.2) \times 10^{-6}$
	298 K			$(1.03 \pm 0.05) \times 10^2$
	$\Delta H_{-3}^{\ddagger}$ (kJ mol^{-1})			131 ± 1
	$\Delta S_{-3}^{\ddagger}$ (J K^{-1} mol^{-1})			235 ± 5
k_{on} (M^{-1} s^{-1}) ($=k_1k_2/k_{-1}$) ($=K_1k_2$)	183 K	$(6.2 \pm 0.5) \times 10^4$ [d]	$(4.32 \pm 0.08) \times 10^3$ [d]	$(7.1 \pm 0.2) \times 10^4$
	223 K	$(6.7 \pm 0.4) \times 10^3$ [d]	$(1.57 \pm 0.02) \times 10^3$ [d]	$(1.1 \pm 0.1) \times 10^5$
	298 K	$(6 \pm 1) \times 10^2$ [d]	$(5.2 \pm 0.2) \times 10^2$ [d]	$(1.8 \pm 0.2) \times 10^5$
	$\Delta H_{on}^{\ddagger}$ (kJ mol^{-1})	-20 ± 2	-10.3 ± 0.2	1.7 ± 0.6
	$\Delta S_{on}^{\ddagger}$ (J K^{-} mol^{-1})	-201 ± 5	-170 ± 1	-139 ± 3

[a] Standard errors of rate constants were calculated from the results of linear regression analyses for the corresponding activation parameters. Rate constants at intermediate temperatures would therefore generally have smaller associated errors than those at the extreme values of 183 and 298 K. [b] Values from ref 41. [c] Relatively uncertain values extrapolated from activation parameters based exclusively on low-temperature data. Calculated uncertainties are close to a factor of 2 at 223 K and 4 at 298 K. [d] Conditional rate constants based on $[(L)Cu(RCN)^+] = 10^{-3}$ M. True second-order rate constants (M^{-1} s^{-1}) are obtained by multiplying the values by 10^3.

$[(D^1)Cu_2(MeCN)_2]^{2+}$ (**2a**) with O_2 initially produces intensely yellow Cu/O_2 = 1:1 superoxo–copper(II) *intermediates* $[(TMPAE)Cu(O_2)]^+$ (**1b′**), $[(D^1)Cu_2(O_2)(EtCN)]^{2+}$ (**2b**), and $[(D^1)Cu_2(O_2)_2]^{2+}$ (**2b′**), described more fully below. These species possess spectral characteristics similar to those of the superoxo–Cu(II) 1:1 adduct $[(TMPA)Cu(O_2)]^+$ (**1b**) (Table 2), previously observed as an intermediate in kinetic studies.[40] Band positions and molar absorptivities for the subsequently formed more stable Cu/O_2 = 2:1 (peroxo)dicopper(II) products $[\{(TMPAE)Cu\}_2(O_2)]^{2+}$ (**1c′**) and $[(D^1)Cu_2(O_2)]^{2+}$ (**2c**) are very close to the values for $[\{(TMPA)Cu\}_2(O_2)]^{2+}$ (**1c**). Calculated spectra of intermediates **1b**, **1b′**, and **2b′**, based on the kinetic analyses presented in the next section, along with products **1c**, **1c′**, and **2c**, are given in Figure 3. Close matching of λ_{max}, ϵ_{max}, and

Table 4. Equilibrium Parameters for O_2 Interaction with Copper(I) Complexes **1a**, **1a′**, and **2a**

		TMPA (**1a**)	TMPAE (**1a′**)	D^1 (**2a**)
K_1 (M^{-1})	183 K	$(1.9 \pm 0.1) \times 10^3$	$(2.84 \pm 0.09) \times 10^2$	$(2.03 \pm 0.04) \times 10^3$
($=k_1/k_{-1}$)	223 K	27 ± 2	6.7 ± 0.4	$(3.2 \pm 0.1) \times 10^1$
	298 K	0.34 ± 0.08	$(9 \pm 1) \times 10^{-2}$	$(2.7 \pm 0.3) \times 10^{-1}$
	$\Delta H_1°$ (kJ mol^{-1})	-34 ± 1	-32 ± 1	-35.3 ± 0.4
	$\Delta S_1°$ (J K^{-1} mol^{-1})	-123 ± 4	-127 ± 3	-129 ± 2
K_2 (−)	183 K	$(2.2 \pm 0.7) \times 10^5$ [a]	$(7 \pm 2) \times 10^5$ [a]	$(9.0 \pm 0.7) \times 10^1$
($=k_2/k_{-2}$)	223 K	$(8.6 \pm 1.2) \times 10^2$ [a]	$(3.7 \pm 0.3) \times 10^3$ [a]	$(9.5 \pm 0.5) \times 10^1$
	298 K	1.5 ± 0.4[a]	8 ± 2[a]	$(1.0 \pm 0.1) \times 10^2$
	$\Delta H_2°$ (kJ mol^{-1})	-47 ± 3	-45 ± 1	0.5 ± 0.6
	$\Delta S_2°$ (J K^{-1} mol^{-1})	-97 ± 10	-76 ± 6	40 ± 3
K_1K_2 (M^{-1})	183 K	$(4.3 \pm 1.5) \times 10^8$ [a]	$(2.1 \pm 0.4) \times 10^8$ [a]	$(1.8 \pm 0.1) \times 10^5$
	223 K	$(2.3 \pm 0.4) \times 10^4$ [a]	$(2.4 \pm 0.1) \times 10^4$ [a]	$(3.0 \pm 0.1) \times 10^3$
	298 K	$(5 \pm 1) \times 10^{-1}$ [a]	$(7 \pm 1) \times 10^{-1}$ [a]	$(2.7 \pm 0.1) \times 10^1$
	$\Delta H_{12}°$ (kJ mol^{-1})	-81 ± 3	-77 ± 1	-34.8 ± 0.4
	$\Delta S_{12}°$ (J K^{-1} mol^{-1})	-220 ± 11	-203 ± 5	-89.3 ± 1.5
K_3[b] (M^{-5})	183 K			3×10^{28}
($=k_3/k_{-3}$)	223 K			$(5 \pm 1) \times 10^{20}$
	298 K			$(4.9 \pm 0.3) \times 10^{11}$
	$\Delta H_3°$ (kJ mol^{-1})			-153 ± 2
	$\Delta S_3°$ (J K^{-1} mol^{-1})			-289 ± 6

[a] Conditional equilibrium constants based on $[(L)Cu(RCN)^+] = 10^{-3}$ M. [b] Minor inconsistencies with Table 3 are due to rounding errors.

band shapes indicates nearly identical structural and electronic characteristics in the corresponding superoxo and peroxo complexes.

Results from benchtop and stopped-flow experiments were identical for the more stable 2:1 species $[\{(TMPAE)Cu\}_2(O_2)]^{2+}$ (**1c′**) and $[(D^1)Cu_2(O_2)]^{2+}$ (**2c**). In addition, with **2a**, a slow secondary rearrangement from **2c** to product(s) **2d**, with similar but definitely distinct spectral features, was observed in the temperature range 203−296 K. The nature of this secondary reaction, which is observed exclusively with the dinuclear complex **2a**, is detailed in the kinetics part of this contribution.

From the very similar spectral features we deduce analogous *trans*-(μ-1,2-peroxo)dicopper(II) structures for complexes **1c**, **1c′**, and **2c**. We note, however, a small but significant shift of $\lambda_{max} = 540$ nm for $[(D^1)Cu_2(O_2)]^{2+}$ (**2c**), to $\lambda_{max} = 525$ nm for $[\{(TMPA)Cu\}_2(O_2)]^{2+}$ (**1c**); a shift in the d−d envelope is also observed (Table 2). We presume this effect to be due to a slightly modified arrangement of the Cu_2O_2 moiety in **2c** with its dinucleating ligand. The detailed kinetics/thermodynamics study of the reaction of O_2 with $[(D^1)Cu_2(MeCN)_2]^{2+}$ (**2a**) provides considerable insight into the nature of the differences between $[\{(TMPA)Cu\}_2(O_2)]^{2+}$ (**1c**) and $[(D^1)Cu_2(O_2)]^{2+}$ (**2c**), as described below.

Stopped-Flow Kinetics/Thermodynamics Investigations

Kinetics of Formation of Superoxo−Copper(II) Cu/O_2 = 1:1 Adducts. Reaction of Mononuclear [(TMPAE)Cu(MeCN)]$^+$ (1a′). Table 3 provides a detailed summary of the kinetics of the reactions of $[(TMPAE)Cu(RCN)^+$ (**1a′**) and $[(D^1)Cu_2(RCN)_2]^{2+}$ (**2a**) with O_2. Rate constants at three temperatures and activation parameters are provided. Published values for $[(TMPA)Cu(RCN)]^+$ are included for comparison. Equilibrium parameters, discussed separately below, are provided in Table 4. As implied by the discussions of UV−vis spectroscopy in the previous section, the O_2-binding behavior of **1a′** is very similar to that of the parent compound [(TMPA)Cu(MeCN)]$^+$ (**1a**). Time-dependent UV−vis spectra of the reaction of [(TMPAE)Cu(MeCN)]$^+$ (**1a′**) with O_2, as well as plots of absorbance versus time at 415 and 532 nm, are given in supporting information Figures S3 and S4. The latter plots correlate perfectly with the kinetic model already presented for the reaction of [(TMPA)Cu(MeCN)]$^+$ (**1a**) with O_2 (Scheme 1),[40] i.e., eqs 4−6. Clearly, the O_2-binding reactivity of the

$$\underset{\mathbf{1a'}}{[(TMPAE)Cu(RCN)]^+} + O_2 \underset{k_{-1}}{\overset{k_1, K_1}{\rightleftharpoons}} \underset{\mathbf{1b'}}{[(TMPAE)Cu(O_2)]^+} + RCN \quad \text{(eq 4)}$$

$$\underset{\mathbf{1a'}}{[(TMPAE)Cu(RCN)]^+} + \underset{\mathbf{1b'}}{[(TMPAE)Cu(O_2)]^+} \underset{k_{-2}}{\overset{k_2, K_2}{\rightleftharpoons}} \underset{\mathbf{1c'}}{[\{(TMPAE)Cu\}_2(O_2)]^{2+}} + RCN \quad \text{(eq 5)}$$

$$\underset{\mathbf{1c'}}{[\{(TMPAE)Cu\}_2(O_2)]^{2+}} \rightarrow \text{irreversible decay} \quad \text{(eq 6)}$$

ester complex [(TMPAE)Cu(MeCN)]$^+$ (**1a′**) closely matches that observed for the parent complex [(TMPA)Cu(MeCN)]$^+$ (**1a**), as revealed by comparisons of (i) spectra shown in Figure 4 and (ii) kinetic parameters in Table 3. The metastable 1:1 Cu−O_2 superoxo−Cu(II) adduct [(TMPAE)Cu(O_2)]$^+$ (**1b′**) forms reversibly ($\lambda_{max} = 415$ nm, $\epsilon = 3330$ M^{-1} cm^{-1}, Table 2). In the temperature range studied, the "on" rate constant (k_1) is about half of that observed for formation of [(TMPA)Cu(O_2)]$^+$ (**1b**). Conversely, the "off" rate constant k_{-1} for **1b′** is twice that for **1b**. Since steric effects should not play a role here, this slower formation and faster decay should reflect the difference in redox potentials in complexes **1a** and **1a′**, in which the TMPA ligand slightly favors Cu(II) relative to Cu(I), compared to TMPAE (cf. Table 1).

It is also interesting to compare O_2-binding kinetics with those of another mononuclear copper(I) complex, [(BQPA)Cu]$^+$, which preferentially forms a 1:1 adduct for steric reasons.[40,49] Such hindrances might be expected to influence the approach of O_2, and [(BQPA)Cu(O_2)]$^+$ forms much more slowly, with $k_1 = 18 \pm 1$ M^{-1} s^{-1} at 183 K.

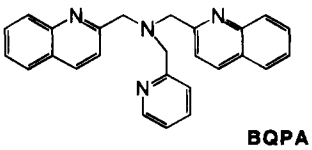

BQPA

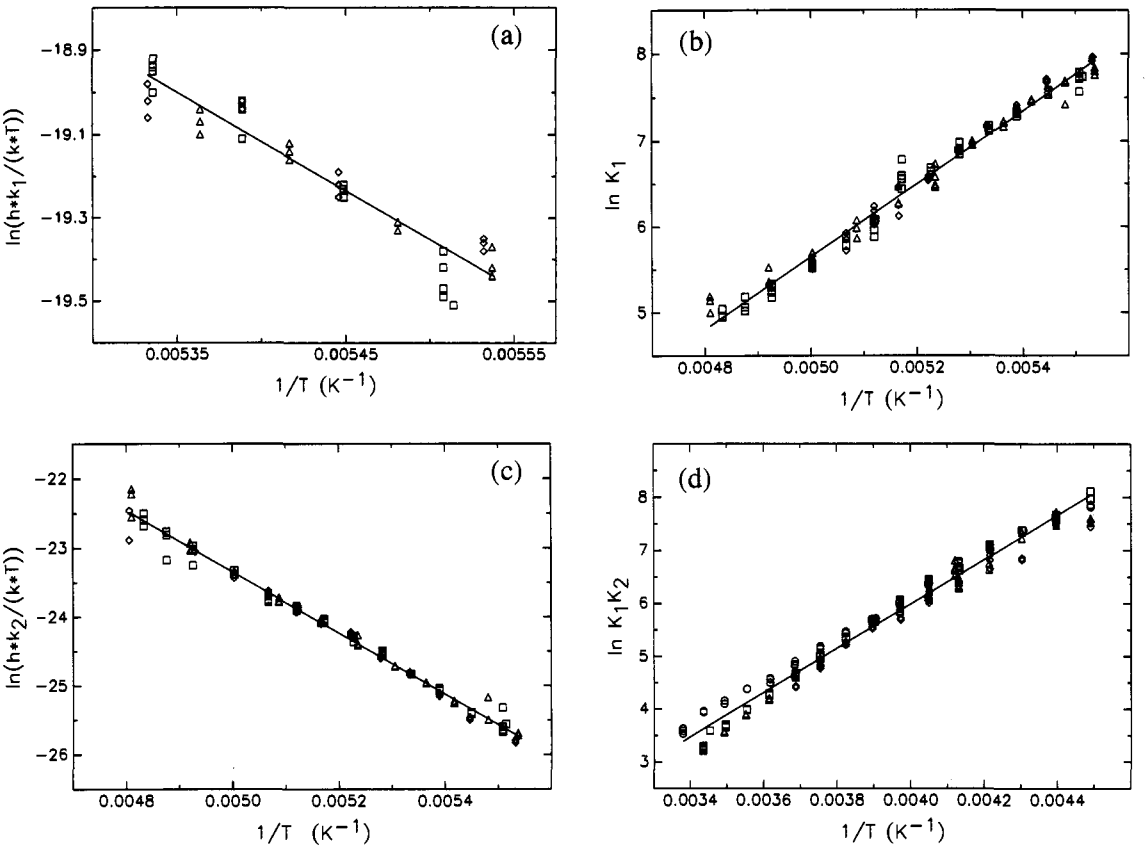

Figure 4. (a) Plot of $\ln[k_1h/(kT)]$ vs $1/T$ (k = Boltzmann constant). $[\{(D^1)Cu_2(MeCN)_2\}^{2+}]/[O_2]$: □, 5.06×10^{-4} M/4.4 × 10^{-3} M; △, 1.28×10^{-4} M/4.4 × 10^{-3} M; ◇, 7.44×10^{-5} M/4.4 × 10^{-3} M. (b) Plot of ln K_1 vs $1/T$. For concentrations, cf. part a. (c) Plot of $\ln[k_2h/(kT)]$ vs $1/T$. For concentrations, cf. part a. (d) Plot of ln K_1K_2 vs $1/T$. $[\{(D1)Cu_2(MeCN)_2\}^{2+}]/[O_2]$: ○, 6.97×10^{-4} M/4.4 × 10^{-3} M; □, 3.21×10^{-4} M/4.4 × 10^{-3} M; △, 1.92×10^{-4} M/4.4 × 10^{-3} M; ◇, 6.52×10^{-5} M/4.4 × 10^{-3} M.

Reaction of Dinuclear $[(D^1)Cu_2(MeCN)_2]^{2+}$ (2a) with O_2. The kinetics of reaction of O_2 with the *dinuclear* complex $[(D^1)Cu_2(MeCN)_2]^{2+}$ (**2a**) are even more complicated than those observed for the mononuclear analogues $[(TMPA)Cu(MeCN)]^+$ (**1a**) and $[(TMPAE)Cu(MeCN)]^+$ (**1a′**). However, detailed analysis has allowed us to deduce a rather complete picture, aided by the assumption (and realization) that the basic elements of the behavior of **1a** and **1a′** should be present in the reaction of **2a** with O_2. Thus, both Cu(I)/O_2 1:1 and 2:1 binding are expected and reactivities of the two individual O_2-binding sites in **2a** would closely match those of **1a** and **1a′**. The relevant kinetic scheme is summarized by the reactions shown in eqs 7−11 (Chart 2). In addition one has to take into account that, because of the dinuclear nature of **2a** with independently reacting Cu(I) units *intermolecular* peroxo species analogous to **1c** or **1c′** will be formed with rate constants close to those observed for **1a** and **1a′**. Plots of (i) time-dependent UV−vis spectra for **2a** + O_2 at 183 K and (ii) experimental and correlated theoretical absorbance versus time plots at 417 nm (following the formation and decay of 1:1 adducts **2b** and **2b′**) and 540 nm (following the formation of 2:1 adduct **2c**) are given as supporting information.[42]

Initial reaction of O_2 with $[(D^1)Cu_2(MeCN)_2]^{2+}$ (**2a**) gives rise to 1:1 dioxygen binding similar to $[(TMPA)Cu(O_2)]^+$ (**1b**) and $[(TMPAE)Cu(O_2)]^+$ (**1b′**), again best observable at the lowest temperatures. However, the presence of *two* equivalent copper(I) sites available in **2a** leads to formation of two such intermediates. Species $[(D^1)Cu_2(O_2)(EtCN)]^{2+}$ (**2b**) is a 2:1 *open* form (eq 7), having one dioxygen coordinated to one copper ion of the dicopper complex. Thus, it is formally a mixed-valence Cu(I)Cu(II)−superoxo species. Intermediate **2b′** is a bis-dioxygen adduct $[(D^1)Cu_2(O_2)_2]^{2+}$, i.e., a 2:2 *open* form, eq 8. These copper−dioxygen adducts both exhibit identical UV−vis λ_{max} = 416 nm, with **2b′** giving the more intense absorption (ϵ = 8900 M^{-1} cm^{-1}) since there are twice the number of absorbing chromophores. Intermediates **2b** and **2b′** cannot be distinguished spectroscopically or kinetically, since the O_2-binding sites are identical and behave independently. **2b′** is, however, a necessary species, since its formation inhibits rapid formation of **2c** from **2b** (eq 9), as especially observed at the lowest temperatures. Thus, while the rate and thermodynamic constants for the initial O_2-binding process (i.e., k_1, k_{-1}, and K_1) which produces **2b** (eq 7) are determined experimentally, the constants k_1' and k_{-1}' (and K_1') (eq 8) were coupled to the former values through statistical factors which led to successful numerical analysis. Specific assumptions and constraints were as follows: (a) The spectrum of 1:1 adduct **2b** is the arithmetic mean of the spectrum of the 2:2 complex **2b′** and the parent Cu(I) species **2a**. (b) $k_1' = 0.5k_1$ and $k_{-1}' = 2k_{-1}$. Plots of temperature dependence yielding activation and thermodynamic parameters for k_1 and K_1, respectively (therefore also providing k_{-1} data), are given in parts a and b, respectively, of Figure 4.

General Observations. For all 1:1 adducts of mononuclear complexes thus far studied [i.e., **1b**,[40] **1b′** (Table 3), and $[(BQPA)Cu(O_2)]^+$],[40] O_2-binding (k_{on}) activation enthalpies are significant ($\Delta H_1^{\ddagger}$ = 30−32 kJ mol^{-1}), while the values ($\Delta H_{-1}^{\ddagger}$ = 63−66 kJ mol^{-1}) associated with the O_2-off reactions (k_{-1}) are much greater. Somewhat different activation parameters are observed for O_2 on or off binding to the dinuclear complex $[(D^1)Cu_2(MeCN)_2]^{2+}$ (**2a**). $\Delta H_1^{\ddagger}$ is lower for **2a**, i.e., 20 kJ mol^{-1} (Table 3). In compensation, $\Delta S_1^{\ddagger} = -53 \pm 6$ J K^{-1} mol^{-1} for O_2 binding to **2a** (eq 7), while the corresponding value for $[(TMPA)Cu(MeCN)]^+$ (**1a**) is $\Delta S_1^{\ddagger} = +14 \pm 18$ J K^{-1}

Chart 2

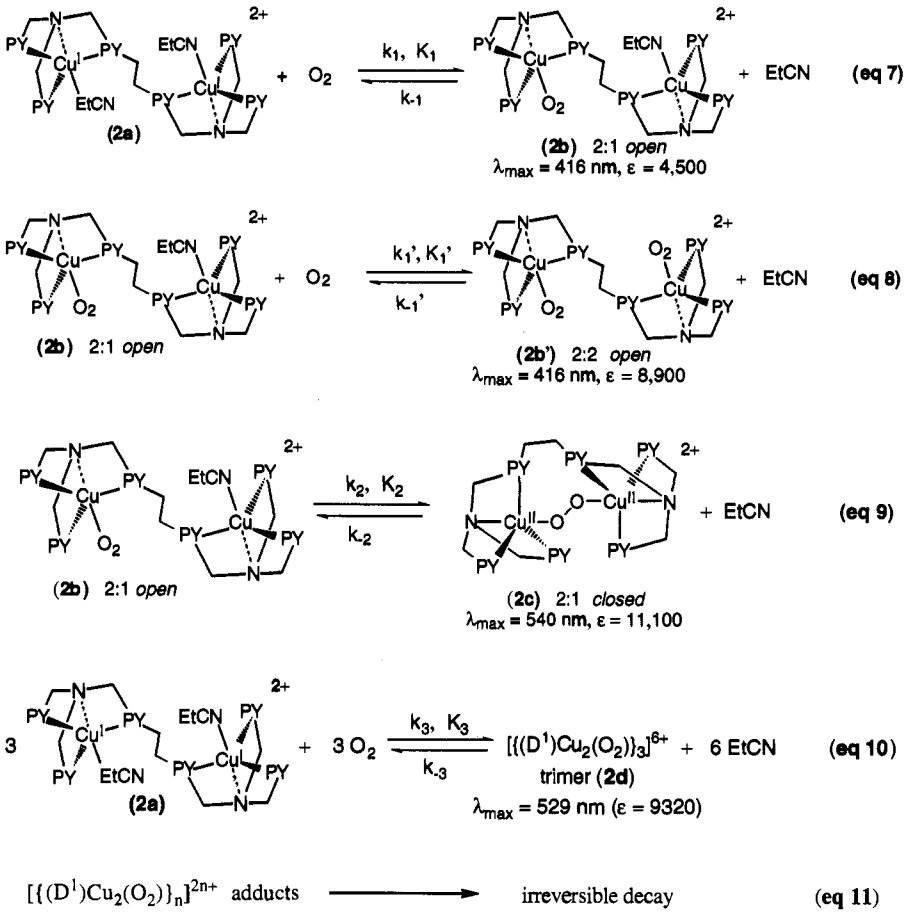

mol^{-1} (Table 3). An explanation for this more negative activation entropy associated with O_2 binding to dinuclear species **2a** is that it reflects the inherently greater number of degrees of freedom for the much bigger and more complex dinuclear complex **2a**, and corresponding changes and organization that will occur during the O_2-binding process. Notable, however, is that the accessible temperature range (180−188 K) for the determination of k_1 is rather limited, the associated standard errors of the activation parameters are considerable, and the absolute values of the directly measured rate constants k_1 for **1a** and **2a** are almost identical, within 90% confidence limits.

Kinetics of Formation of (μ-Peroxo)copper(II) Cu/O_2 = 2:1 Adducts. Formation of [{(TMPAE)Cu}$_2$(O_2)]$^{2+}$ (1c'). As discussed above and illustrated in Figure 3b, the distinctive charge-transfer bands in the UV−vis region observed for [{(TMPAE)Cu}$_2$(O_2)]$^{2+}$ (**1c'**) closely match those of the X-ray structurally characterized complex [{(TMPA)Cu}$_2$(O_2)]$^{2+}$ (**1c**), implicating congruent *trans*-(μ-1,2-peroxo)dicopper(II) structures for both of the species derived from mononuclear precursors [(TMPA)Cu(MeCN)]$^+$ (**1a**) or [(TMPAE)Cu(MeCN)]$^+$ (**1a'**).

The final Cu_2O_2 2:1 (peroxo)dicopper(II) complex [{(TMPAE)-Cu}$_2$(O_2)]$^{2+}$ (**1c'**) forms by further reversible reaction of [(TMPAE)Cu(O_2)]$^+$ (**1b'**) with **1a'** (eq 5). Again, while overall similar formation rates (and thermodynamic effects, vide infra) are observed, a detailed examination shows that **1c'** is formed up to 15 times more slowly at 183 K than is the "parent" analogue [{(TMPA)Cu}$_2$(O_2)]$^{2+}$ (**1c**), Table 3. Differences are less at higher temperatures. In fact, calculated rates are about equal at 298 K. Significantly, "off" values k_{-2} for **1c'** are smaller than or equal to those for **1c**. The k_{on} ($=K_1k_2$) value for [{(TMPAE)Cu}$_2$(O_2)]$^{2+}$ (**1c'**) is quite close to that found for the formation of a spectroscopically similar peroxo−dicopper(II) complex, [{(BPQA)Cu}$_2$(O_2)]$^{2+}$, for which k_{on} = (3.2 ± 0.1) × 10^6 M^{-2} s^{-1} at 183 K.[40] Investigations of compounds possessing systematically varied electronic properties and steric differences are needed to better understand precisely what contributes to and controls Cu_n−O_2 complex formation and stability.

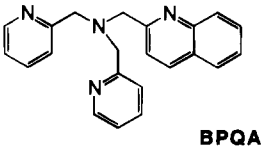

BPQA

Formation of μ-Peroxo [(D^1)Cu$_2$(O_2)]$^{2+}$ (2c). Following the formation of the 1:1 adducts **2b** and **2b'**, the ensuing product is the 2:1 *closed* (μ-peroxo)dicopper(II) complex [(D^1)Cu$_2$-(O_2)]$^{2+}$ (**2c**) (eq 9), identified by the kinetics (i.e., concentration dependences) and spectral characteristics (vide supra), λ_{max} = 540 nm (ϵ = 11 100 M^{-1} cm^{-1}), 600 (sh) nm. The gross similarities with [{(TMPA)Cu}$_2$(O_2)]$^{2+}$ (**1c**) and [{(TMPAE)-Cu}$_2$(O_2)]$^{2+}$ (**1c'**) (Figure 3b) suggest that a *trans*-(μ-1,2-peroxo)dicopper(II) intramolecular structure (as depicted in eq 9) is formed, consistent with our examination of hand-held molecular models and the subsequent design of D^1 with its −CH_2CH_2− linker. This complex forms directly from the 2:1 *open* Cu(I)Cu(II)−superoxo complex [(D^1)Cu$_2$(O_2)(EtCN)]$^{2+}$ (**2b**) (eq 9). Very low temperatures and/or excess O_2 inhibits the formation of μ-peroxo **2c** by favoring formation of bis-O_2 intermediate [(D^1)Cu$_2$(O_2)$_2$]$^{2+}$ (**2b'**, eq 8), where both copper sites are blocked. The formation of [(D^1)Cu$_2$(O_2)]$^{2+}$ (**2c**) is

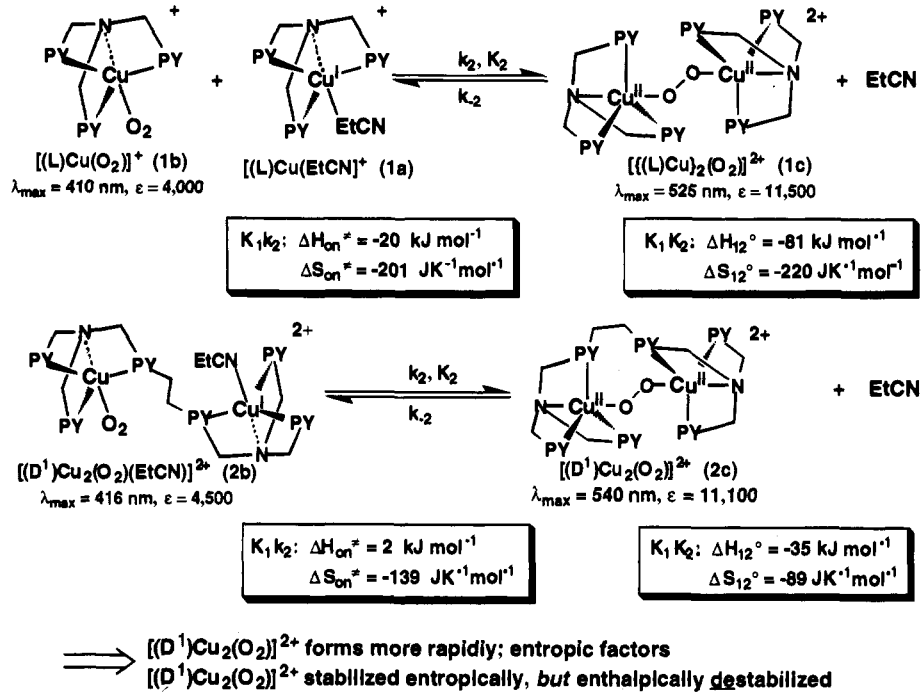

Figure 5. Comparisons of kinetic and thermodynamic parameters for overall formation of (peroxo)dicopper(II) dinuclear adducts **1c** and **2c** from copper(I) precursors.

described by the rate and equilibrium constants k_2, k_{-2}, and K_2 and the second-order rate constant $k_{on} = K_1k_2$, while K_1K_2 represents the overall equilibrium formation of **2c** from **2a**. Plots for the temperature dependence of k_2 and K_1K_2 are given in parts c and d, respectively, of Figure 4, and the results of numerical analysis giving kinetic and thermodynamic parameters pertaining to **2c** formation are found in Tables 3 and 4.

The *intramolecular* formation of $[(D^1)Cu_2(O_2)]^{2+}$ (**2c**) is significantly more rapid than for the corresponding 2:1 complexes $[\{(TMPA)Cu\}_2(O_2)]^{2+}$ (**1c**) and $[\{(TMPAE)Cu\}_2(O_2)]^{2+}$ (**1c′**), the latter being formed in an *intermolecular* fashion from their mononuclear precursors. At 213 K, **2c** formation is already beyond the experimental limit (~8 ms) of the stopped-flow instrument. For comparisons, Figure 5 provides pertinent kinetic and equilibrium parameters for **2c** formation from dicopper(I) precursor $[(D^1)Cu_2(EtCN)_2]^{2+}$ (**2a**), and corresponding parameters for $[\{(TMPA)Cu\}_2(O_2)]^{2+}$ (**1c**) generation by reaction of mononuclear $[(TMPA)Cu(EtCN)]^+$ (**1a**) with $[(TMPA)Cu(O_2)]^+$ (**1b**).

Pertaining to the individual kinetic step k_2 (i.e., where a Cu–O_2 1:1 intermediate attacks a second Cu–EtCN species), there is a substantially higher activation enthalpy for formation of $[(D^1)Cu_2(O_2)]^{2+}$ (**2c**) (eq 9) relative to $[\{(TMPA)Cu\}_2(O_2)]^{2+}$ (**1c**) (eq 2): $\Delta H_2^{\ddagger} = 37$ and 14 kJ mol^{-1} for **2c** and **1c**, respectively. This is, however, well overcompensated by a dramatic change in activation entropy: $\Delta S_2^{\ddagger} = -9$ and -78 J K^{-1} mol^{-1} for **2c** and **1c**, strongly favoring formation of **2c** over **1c** on a kinetic basis.

For direct comparison of the intra- versus intermolecular process occurring in the formation of $[(D^1)Cu_2(O_2)]^{2+}$ (**2c**) versus $[\{(TMPA)Cu\}_2(O_2)]^{2+}$ (**1c**) or $[\{(TMPAE)Cu\}_2(O_2)]^{2+}$ (**1c′**), Table 3 also provides pseudo-first-order rate constants for k_2 and k_{on} (K_1k_2), calculated at $[\{(tripod\text{-}ligand)Cu^I(RCN)\}^+] = 10^{-3}$ M, since the orders of the overall reactions differ. At the intermediate temperature of 223 K, k_2 and k_{on} are ~13–16 times greater for the process involving intramolecular **2c** formation. The difference is smaller at lower temperatures, while it is greater at higher temperatures. Comparisons between **2c** and **1c′** formation (Table 3) actually indicate even greater differences in these two systems.

Strong entropic support of intramolecular peroxo formation in **2c** relative to **1c** is also evident from the overall rate constant k_{on}: $\Delta S_{on}^{\ddagger} = -139$ J K^{-1} mol^{-1} vs -201 J K^{-1} mol^{-1} (cf. Figure 5). This is combined with a small positive activation enthalpy $\Delta H_{on}^{\ddagger} = 1.7 \pm 0.6$ kJ mol^{-1} associated with the overall rate constant k_{on} ($=K_1k_2$, Table 3), contrary to what is observed for formation of $[\{(TMPA)Cu\}_2(O_2)]^{2+}$ (**1c**), $[\{(TMPAE)Cu\}_2(O_2)]^{2+}$ (**1c′**), and $[\{(BPQA)Cu\}_2(O_2)]^{2+}$,[40] where negative overall activation enthalpies are found for this composite parameter, since the value of $\Delta H_{-1}^{\ddagger}$ exceeds that of $\Delta H_1^{\ddagger}$ and $\Delta H_2^{\ddagger}$ combined. Thus, for $[(D^1)Cu_2(O_2)]^{2+}$ (**2c**), k_{on} increases with increasing temperature. However, the larger value of $\Delta H_{on}^{\ddagger}$ (+2 versus -20 kJ mol^{-1}) is suggestive of a structurally "strained" transition state.

An examination of the k_{-2} ($=k_{off}$) values and associated activation parameters (Table 3) provides further insight into the strained nature of $[(D^1)Cu_2(O_2)]^{2+}$ (**2c**). These values describe the disruption, i.e., dissociation of O_2 from **2c** (eq 9), and they can also be compared to corresponding ones for mononuclear species $[\{(TMPA)Cu\}_2(O_2)^{2+}$ (**1c**) or $[\{(TMPAE)Cu\}_2(O_2)]^{2+}$ (**1c′**) (eqs 2 and 5, Figure 5, and Table 3). At 223 K, the rate constant for breakage of one of the copper–oxygen bonds in the Cu–O_2–Cu group of $[(D^1)Cu_2(O_2)]^{2+}$ (**2c**) giving $[(D^1)Cu_2(O_2)(EtCN)]^{2+}$ (**2b**) is 3.5 ($\pm$0.2) $\times$ 10^1 s^{-1}, ~120 times greater than the corresponding value for $[\{(TMPA)Cu\}_2(O_2)]^{2+}$ (**1c**), and greater than that found for $[\{(TMPAE)Cu\}_2(O_2)]^{2+}$ (**1c′**). Correspondingly for **2c** → **2b** (eq 9), $\Delta H_{-2}^{\ddagger} = 37 \pm 1$ kJ mol^{-1}, compared to a range of 61–66 kJ mol^{-1} for related processes **1c** → **1b** + **1a**, or **1c′** → **1b′** + **1a′**. The negative activation entropy ascribed to this disruptive bond-breaking process for the dinuclear case $[(D^1)Cu_2(O_2)]^{2+}$ (**2c**) → $[(D^1)Cu_2(O_2)(EtCN)]^{2+}$ (**2b**) is $\Delta S_{-2}^{\ddagger} = -49 \pm 3$ J K^{-1} mol^{-1}, suggesting an early transition state where EtCN solvent attacks the intact peroxo–dicopper(II) complex (eq 9), giving the single-molecule product **2b**. However, the $\Delta S_{-2}^{\ddagger}$ values are positive, 19 and 33 J K^{-1} mol^{-1}, for the breaking of Cu_2–O_2 moieties composed of mononuclear components, i.e., **1c** → **1b** and **1c′**

→ **1b′**, respectively, in these cases two molecules (i.e., EtCN and the dinuclear complexes **1c** or **1c′**) combine to form two molecules $[(TMPA)Cu(O_2)]^+$ (**1b**) (or **1b′**) plus $[(TMPA)Cu(EtCN)]^+$ (**1a**) (or **1a′**).

Thermodynamics. Table 4 provides equilibrium parameters for O_2 binding to mono- or dinuclear copper(I) complexes of TMPA, TMPAE, and D^1.

Superoxo−Copper(II) Cu/O_2 = 1:1 Adducts. General observations are that for all 1:1 adducts thus far studied, i.e., $[(TMPA)Cu(O_2)]^+$ (**1b**), $[(TMPAE)Cu(O_2)]^+$ (**1b′**), $[(D^1)Cu_2(O_2)(EtCN)]^{2+}$ (**2b**), and $[(BQPA)Cu(O_2)]^+$,[40] there is a remarkable similarity in the thermodynamics of O_2-binding parameters. The stability of dioxygen binding to a single copper(I) ion site is driven by favorable enthalpies ($\Delta H_1° = -32$ to -35 kJ mol^{-1}), but unfavorable entropies ($\Delta S_1° = -123$ to -129 J K^{-1} mol^{-1}) preclude observation of $Cu-O_2$ (and Cu_2-O_2) complexes at ambient temperatures.[9]

Some individual comparisons are interesting, such as in the relative stabilities of $[(TMPA)Cu(O_2)]^+$ (**1b**) versus $[(TMPAE)Cu(O_2)]^+$ (**1b′**). The thermodynamic binding constant K_1 is a factor of 4−7 times less for the latter at low temperatures. As mentioned (vide supra) with reference to the kinetics, since steric effects in binding of O_2 to $[(TMPA)Cu(EtCN)]^+$ (**1a**) versus $[(TMPAE)Cu(EtCN)]^+$ (**1a′**) should be unimportant, this variation in K_1 should reflect the slightly more positive Cu(I)/Cu(II) complex redox potential observed for **1a′** [$E_{1/2} = -608$ (**1a**), -550 mV (**1a′**) in DMF vs Ag/AgNO$_3$, Table 1];[70] i.e., there is a smaller driving force toward the redox reaction producing a superoxo−copper(II) product from O_2 and LCu(I).

On the other hand, $[(BQPA)Cu(O_2)]^+$ has a thermodynamic stability [$K_1 = (2.9 \pm 0.3) \times 10^3$ M^{-1} at 183 K, $\Delta H_1° = -35 \pm 6$ kJ mol^{-1}, $\Delta S_1° = -125 \pm 27$ J K^{-1} mol^{-1}] quite comparable to that for $[(TMPA)Cu(O_2)]^+$ (**1b**) or $[(TMPAE)Cu(O_2)]^+$ (**1b′**) in spite of the reduced driving force for the oxidation of $[(BQPA)Cu]^+$ (relative to **1a** and **1a′**, cf. Table 1; $E_{1/2} = -0.410$ mV in DMF vs Ag/AgNO$_3$).[49] Detailed studies on a larger collection of compounds will be required to more fully understand how the formation rates and thermodynamics of copper−dioxygen complexes are controlled by (i) ligand electronic variations and (ii) ligand environment or steric effects.

While thermodynamic parameters K_1, $\Delta H_1°$, and $\Delta S_1°$ for 1:1 O_2 binding to dinuclear $[(D^1)Cu_2(RCN)_2]^{2+}$ (**2a**) (Table 4) are similar to those observed for $[(TMPA)Cu(MeCN)]^+$ (**1a**) and $[(TMPAE)Cu(MeCN)]^+$ (**1a′**) (Table 4), they are closer to those for **1a**; differences between **1a** and **2a** are, in fact, statistically insignificant. Apparently, the $-CH_2CH_2-$ chain substituent on the 5-position of one pyridyl group in **2a** gives a complex more similar to the parent complex **1a** (with H in this position) than is the case for **1a′**, where the electronic structure could be more affected by the 5-ester group (Chart 1). The electrochemically determined redox potentials for the copper(I) complexes **1a**, **1a′**, and **2a** (Table 1) support this conclusion; $E_{1/2}$ values for **1a** and **2a** are quite close, while that for **1a′** is more positive.

As discussed (vide supra) and displayed in Figure 3a (with data given in Table 2), the UV−vis spectra of 1:1 $Cu-O_2$ intermediates $[(TMPA)Cu(O_2)]^+$ (**1b**), $[(TMPAE)Cu(O_2)]^+$ (**1b′**), and $[(D^1)Cu_2(O_2)(EtCN)]^{2+}$ (**2b**) are similar. While these comparisons suggest that they have the *same* coordination, the detailed structure of these superoxo−copper(II) species is not known. We have discussed[40,49,71] the possibilities, i.e., η^2 side-on binding, or "terminal" end-on $Cu^{II}-O-O^-$ ligation. The

former is known for a superoxo−cobalt(II) complex (formed from O_2 reaction with a Co(I) complex) possessing a sterically demanding hydrotris(3-*tert*-butyl-5-methylpyrazolyl)borate ligand;[72] η^2-O_2 ligation is also observed in $Cu(O_2)(HB(3-t\text{-}Bu\text{-}5\text{-}i\text{-}Prpz)_3)$ [HB(3-*t*-Bu-5-*i*Prpz)$_3$ = hydrotris(3-*tert*-butyl-5-isopropyl)pyrazolylborate].[29] Physical−spectroscopic data for these Co and Cu complexes are consistent with the superoxo−metal(II) formulation; thus, substantial electron transfer from M(I) to O_2 has occurred upon dioxygen binding. An "end-on" coordination is observed in a superoxo−Cu(II) species which is an analogue of TMPA with 6-pivaloylamine substituents on the pyridyl groups; hydrogen bonding by proximal N−H amide groups of this ligand is suggested to stabilize the structure described.[30] Analogy to this latter complex and the observed overwhelming tendency for pentacoordination in copper(II) complexes with these kinds of tetradentate ligands[71] would suggest end-on superoxo coordination in $[(TMPA)Cu(O_2)]^+$ (**1b**), $[(TMPAE)Cu(O_2)]^+$ (**1b′**), and $[(D^1)Cu_2(O_2)(EtCN)]^{2+}$ (**2b**). Further structural and spectroscopic studies are needed.

(μ-Peroxo)copper(II) Cu/O_2 = 2:1 Adducts. As for the formation of 1:1 adducts, parameters K_2 and $\beta_2 = K_1K_2$ for formation of μ-peroxo complexes $[\{(TMPA)Cu\}_2(O_2)]^{2+}$ (**1c**) and $[\{(TMPAE)Cu\}_2(O_2)]^{2+}$ (**1c′**) are quite similar. The TMPAE adduct **1c′** is a factor of ~2 less stable at 183 K (Table 4), but at 223 K the values are identical. Also based on values at 183 K, both **1c** [$\beta_2 = (4.3 \pm 1.5) \times 10^{11}$ M^{-2}] and **1c′** $\beta_2 = (2.1 \pm 0.4) \times 10^{11}$ M^{-2}) are thermodynamically more stable than the quinolyl-substituted 2:1 complexes $[\{(BPQA)Cu\}_2(O_2)]^{2+}$ [$\beta_2 = (1.7 \pm 0.2) \times 10^{10}$ M^{-2}] or $[\{(BQPA)Cu\}_2(O_2)]^{2+}$ [$\beta_2 = (6 \pm 12) \times 10^6$ M^{-2}].[40] Again, investigations of compounds possessing well-defined, but systematically varied, electronic properties and steric differences are needed to better understand precisely what contributes to and controls Cu_n-O_2 complex formation and stability.

Comparisons of the overall thermodynamics for the reaction

$$\underset{\textbf{2a}}{[(D^1)Cu_2(RCN)_2]^{2+}} + O_2 \rightarrow \underset{\textbf{2c}}{[(D^1)Cu_2(O_2)]^{2+}}$$

vs

$$\underset{\textbf{1a}}{2[(TMPA)Cu(RCN)]^+} + O_2 \rightarrow \underset{\textbf{1c}}{[\{(TMPA)Cu\}_2(O_2)]^{2+}}$$

are most revealing (Figure 5). As expected from the original concept and design of a dinucleating analogue D^1, the *intramolecular* process provides considerable entropic stabilization of $[(D^1)Cu_2(O_2)]^{2+}$ (**2c**) compared to $[\{(TMPA)Cu\}_2(O_2)]^{2+}$ (**1c**), $\Delta S_{12}° = -89$ vs -220 J K^{-1} mol^{-1}. However, *no* real stabilization of peroxo complex **2c** occurs. In fact, $\Delta G°$ is less negative for dinucleating ligand complex $[(D^1)Cu_2(O_2)]^{2+}$ (**2c**) compared to **1c** over the entire range 183−298 K, because of the dramatic enthalpic *destabilization* in forming $[(D^1)Cu_2(O_2)]^{2+}$ (**2c**) compared to $[\{(TMPA)Cu\}_2(O_2)]^{2+}$ (**1c**), $\Delta H_{12}° = -35$ vs -81 kJ mol^{-1}, respectively. This overall destabilization of **2c** relative to **1c** is entirely due to the second step K_2, which in fact has no significant binding enthalpy (0.5 kJ mol^{-1})

(70) $E_{1/2} = -350$ (**1a**), -300 mV (**1a′**) in MeCN vs Ag/AgNO$_3$, unpublished results.

(71) Wei, N.; Murthy, N. N.; Karlin, K. D. *Inorg. Chem.* **1994**, *33*, 6093−6100.

(72) Egan, J. W.; Haggerty, B. S.; Rheingold, A. L.; Sendlinger, S. C.; Theopold, K. H. *J. Am. Chem. Soc.* **1990**, *112*, 2445−2446.

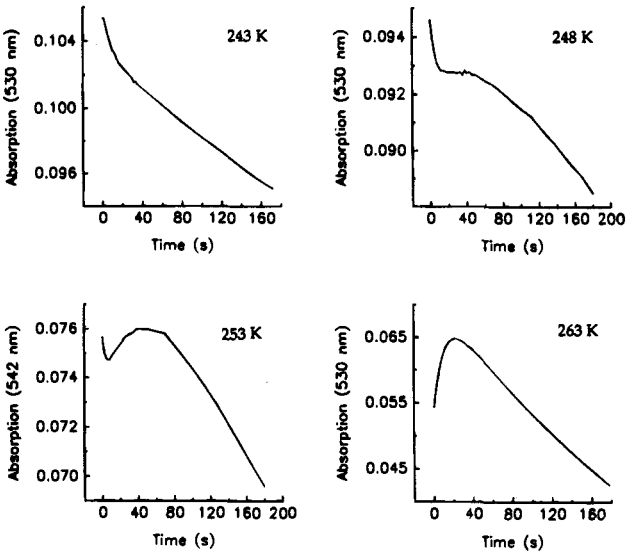

Figure 6. Kinetics of secondary reaction of $[(D^1)Cu_2(O_2)]^{2+}$ at several temperatures.

for **2c** but rather substantial ones, −47 and −45 kJ mol^{-1}, for **1c** and **1c′**, respectively.

As argued, we ascribe the destabilization of $[(D^1)Cu_2(O_2)]^{2+}$ (**2c**) compared to $[\{(TMPA)Cu\}_2(O_2)]^{2+}$ (**1c**) or $[\{(TMPAE)Cu\}_2(O_2)]^{2+}$ (**1c′**) to the formation of a "strained" metastable peroxo−dicopper(II) structure **2c**. Our design of D^1-complex/O_2 chemistry anticipated that a structure strictly analogous to **1c** and **1c′** should form, but there are significant differences in the details of the Cu_2-O_2 coordination environment and stability caused by the presence of a $-CH_2CH_2-$ moiety linking the two halves of the molecule. Further evidence for this comes from the differences in vis spectra of **2c**, compared to **1c** and **1c′**, Table 2. There is a clear bathochromic shift in the charge-transfer (LMCT) absorption maximum for $[(D^1)Cu_2(O_2)]^{2+}$ (**2c**) (Figure 4b), $\lambda_{max} = 540$ nm ($\epsilon = 11\,100$), since for $[\{(TMPA)Cu\}_2(O_2)]^{2+}$ (**1c**) $\lambda_{max} = 525$ nm ($\epsilon = 11\,500$) and for $[\{(TMPAE)Cu\}_2(O_2)]^{2+}$ (**1c′**) $\lambda_{max} = 532$ nm ($\epsilon = 9380$). We have previously observed significant differences in the charge-transfer band position and intensity in Cu_2-O_2 complexes with variably linked $-(CH_2)_n-$ ($n = 3-5$) bis[2-(2-pyridyl)ethyl]-amine units,[58] indicating the sensitivity of such absorptions to local environment. A further indication that the coordination environment about the Cu(II) ions in **2c** may be altered compared to **1c** is that there is a small but significant shift in the position of the d−d bands, $\lambda_{max} = 1010$ and 1035 nm, for **2c** and **1c**, respectively (Table 2).

The conclusion that $[(D^1)Cu_2(O_2)]^{2+}$ (**2c**) possesses a strained structure is also borne out by the fact that it is not the ultimate thermodynamic product of reaction of $[(D^1)Cu_2(RCN)_2]^{2+}$ (**2a**) with O_2, but rearranges to oligomeric peroxo−dicopper(II) products (vide infra).

Formation of Oligomeric *Intermolecular* μ-Peroxo Copper−Dioxygen Adducts. Over the temperature range 203 K to room temperature, the peroxo−copper product from $[(D^1)Cu_2(RCN)_2]^{2+}$ (**2a**) + O_2 is more persistent than is the corresponding analogue $[\{(TMPA)Cu\}_2(O_2)]^{2+}$ (**1c**), but it is not the same species $[(D^1)Cu_2(O_2)]^{2+}$ (**2c**) as that seen at low temperature. Figure 6 provides examples of the kinetics of this secondary rearrangement process, at several temperatures. The spectral change monitored is that for **2c** with $\lambda_{max} = 540$ nm to species characterized by $\lambda_{max} = 529$ nm and $\epsilon = 9320$ M^{-1} cm^{-1} per peroxo unit.

The spectral characteristics indicate that the species formed in this secondary rearrangment also are (peroxo)dicopper(II) species. The kinetic data can be explained in terms of the relief of the strain in $[(D^1)Cu_2(O_2)]^{2+}$ (**2c**), as described above. Thermodynamically more stable oligomeric (peroxo)dicopper-(II) complexes can be formed via a corresponding *intermolecular* process, since the resulting Cu_2-O_2 species no longer suffer from the steric constraints imposed by the $-CH_2CH_2-$ linker, cf. Scheme 4. Such oligomers thus could possess a LMCT absorption close to those found in the unstrained complexes $[\{(TMPA)Cu\}_2(O_2)]^{2+}$ (**1c**) ($\lambda_{max} = 525$ nm) and $[\{(TMPAE)-Cu\}_2(O_2)]^{2+}$ (**1c′**) ($\lambda_{max} = 532$ nm), as observed. Thus, one can conclude that, following the rapid formation of **2c**, a slower rearrangement occurs via the 2:1 open species $[(D^1)Cu_2(O_2)-(EtCN)]^{2+}$ (**2b**), whereupon *intermolecular* reactions (undoubtedly proceeding through intermediates such as **Int**, Scheme 4) lead to more stable (peroxo)dicopper(II) $\{Cu_2-O_2\}_n$ oligomers, Scheme 4. For a number of other cases in copper−dioxygen complex chemistry, Cu_2-O_2 species formed in an intermolecular fashion from dinuclear precursors have previously been postulated in the literature.[35,36,73-75] Although detailed structures are not available, partial data for the kinetics of formation are available in one case.[73,74] A mixed-valent tetrairon $\eta^2:\eta^2$-peroxide-bridged intermediate or transition state has been suggested in the reaction of O_2 with a diiron(II) complex.[4]

The oligomerization process must be quite complex. "Linear" oligomers of varying nuclearity might form. On the basis of the known reactivity of $[(TMPA)Cu(RCN)]^+$, such species would not be sufficiently stable at the higher temperatures studied. However, in the stopped-flow kinetic analysis, we have been fortunate to discern that one particular species, a trimer, $[\{(D^1)Cu_2(O_2)\}_3]^{6+}$ (**2d**), appears especially stable between 266 and 295 K, and the kinetics and thermodynamics of this reaction, eq 10, could be followed and analyzed. Figure 7 shows the Eyring plot for k_3, for the rate of formation of the trimer complex **2d**, from $[(D^1)Cu_2(EtCN)_2]^{2+}$ (**2a**) (eq 10). A corresponding plot for the kinetic constant k_{-3} is provided in the supporting information (Figure S5). For temperatures in the above range, the variable concentration and temperature data, as well as the analysis of the individual experiments, strongly suggest trimer formation. None of several other models, specifically invoking dimers and/or monomers only, were compatible with the data. At lower temperatures, larger oligomers appear to be favored, and since these are more strongly concentration dependent, deviations in the behavior of the k_3 plots occur, i.e., conditional rate constants pertaining to high analytical concentrations become larger than those from dilute solutions.

This trimer species $[\{(D^1)Cu_2(O_2)\}_3]^{6+}$ (**2d**) is remarkably robust and undoubtedly has a closed cyclic architecture; it must be preferentially formed because of some particular stabilization of its structure. A stable "open" form species (e.g., such as **Int**, Scheme 4) with $Cu-O_2$ moieties at one end is excluded, since (i) characteristic spectra (vide supra) of such $Cu/O_2 = 1:1$ entities would have been seen, and (ii) they would not be stable at these higher temperatures. "Open" forms (with internal intermolecular μ-peroxo units) but *without* O_2 at the ends, e.g., $(RCN)Cu-\{(D^1)Cu-(O_2)-Cu(D^1)\}_n-Cu(RCN)$, have also been tested, but their inclusion cannot explain the observed stability of the high-temperature species. We see from Table 4 that the equilibrium constant for formation of **2d** is $K_3 = 3 \times 10^{28}$ M^{-5} at 183 K, with $\Delta H_3° = -153$ kJ mol^{-1} and $\Delta S_3° = -289$ J K^{-1} mol^{-1}.

(73) El-Sayed, M.; Ismail, K. Z.; El-Zayat, T. A.; Davies, G. *Inorg. Chim. Acta* **1994**, *217*, 109−119.
(74) Davies, G.; El-Sayed, M. A.; Henary, M. *Inorg. Chem.* **1987**, *26*, 3266−3273.
(75) Bulkowski, J. E.; Summers, W. E., III. In *Copper Coordination Chemistry: Biochemical & Inorganic Perspectives*; Karlin, K. D., Zubieta, J., Eds.; Adenine Press: Guilderland, NY, 1983; pp 445−456.

Scheme 4

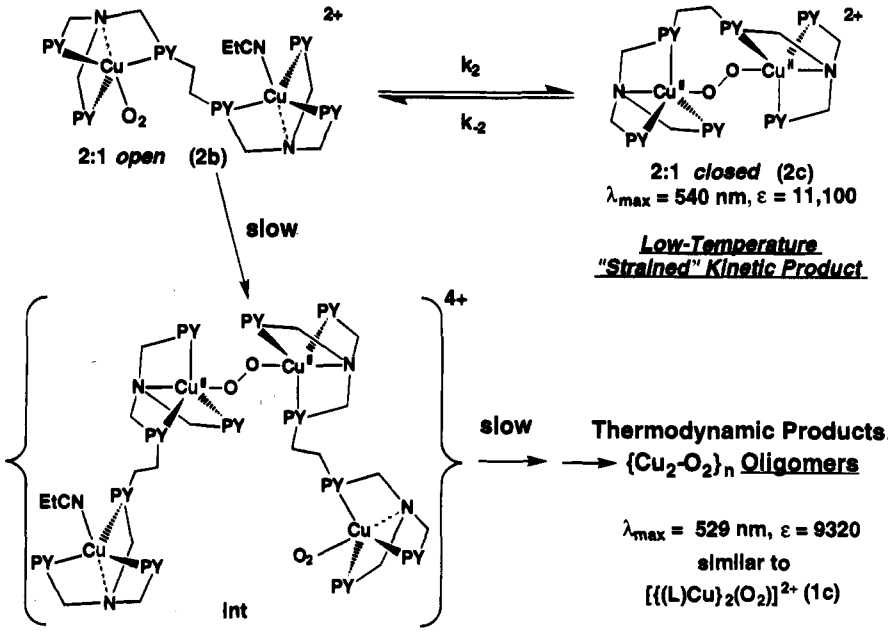

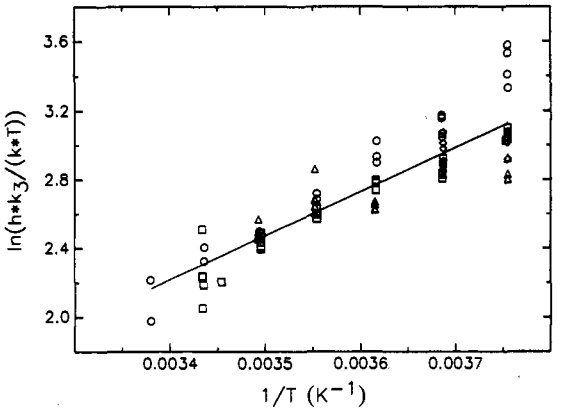

Figure 7. Plot of $\ln[k_3h/(kT)]$ vs $1/T$, k = Boltzmann constant. For concentrations, cf. Figure 4d.

It is interesting to note that the enthalpy of formation of **2d**, when evaluated on the basis of per Cu/O_2 = 2:1 moiety, lies between those for the (peroxo)dicopper(II) moieties in the related species $[\{(TMPA)Cu\}_2(O_2)]^{2+}$ (**1c**) and $[(D^1)Cu_2(O_2)]^{2+}$ (**2c**). The differences in the $\Delta H°$ values (Table 4) are substantial and statistically significant. Thus, $\Delta H_{12}° = -81$ kJ mol^{-1} for the most (enthalpically) stable unstrained system $[\{(TMPA)Cu\}_2(O_2)]^{2+}$ (**1c**), but $\Delta H_3° = (-153$ kJ mol$^{-1})/3 = -51$ kJ mol^{-1} per Cu_2-O_2 unit in the trimer complex $[\{(D^1)Cu_2(O_2)\}_3]^{6+}$ (**2d**), and $\Delta H_{12}° = -34.8$ kJ mol^{-1} for $[(D^1)Cu_2(O_2)]^{2+}$ (**2c**). Thus, intramolecularly formed (peroxo)dicopper(II) complex **2c** is the most strained; it forms rapidly but rearranges to a cyclic trimer in which much, but not all, strain is released relative to that found in the parent system $[\{(TMPA)Cu\}_2(O_2)]^{2+}$ (**1c**). It is interesting to note that the λ_{max} of the charge-transfer transition for these three species also occurs in the same order, i.e., λ_{max} = 540, 529, and 525 nm for **2c**, **2d**, and **1c**, respectively.

Summary and Conclusions

A detailed understanding of dioxygen interactions with copper(I) centers is important in metal-mediated oxidative transformations of organics, and in the biochemistry of copper, possibly extending to metal-promoted oxygen-radical toxicity. Yet, only a few chemical systems involving well-defined copper complexes have been studied.[7,9] Here, we have compared $[(TMPA)Cu(MeCN)]^+$ (**1a**) with two new complexes, $[(TMPAE)Cu(MeCN)]^+$ (**1a′**) and a dinuclear analogue $[(D^1)Cu_2(RCN)_2]^{2+}$ (**2a**). Complex **1a′** forms a Cu_2O_2 peroxo adduct with formation and product characteristics nearly identical to that found for **1a**. Our anticipation that a closely related Cu_2-O_2 peroxo complex would form from **2a** was borne out. However, our expectation that the rapidly formed adduct $[(D^1)Cu_2(O_2)]^{2+}$ (**2c**) would be actually more stable than analogues $[\{(TMPA)Cu\}_2(O_2)]^{2+}$ (**1c**) or $[\{(TMPAE)Cu\}_2(O_2)]^{2+}$ (**1c′**) was not borne out. Thus, **1c** and **1c′** are thermodynamically favored over **2c** with the exception of the extrapolated values at 298 K, where entropic contributions are decisive, but all complexes have no significant stability.

Our investigations of the new compounds **1a′** and **2a** further support our general conclusions[9,40,41] that the formation of copper–dioxygen adducts is kinetically favorable; in fact, the on rates for O_2 binding compare well with those for copper–protein systems.[40,76] Formation enthalpies indicate strong O_2 binding, in the narrow range $\Delta H_1° = -32$ to -35 kJ mol^{-1} for Cu/O_2 = 1:1 complexes [i.e., superoxo–Cu(II) species] with these tripodal tetradentate chelators TMPA, TMPAE, BQPA, and D^1, while $\Delta H_{12}° = -50$ to -81 kJ mol^{-1} for 2:1 Cu_2-O_2 (peroxo)dicopper(II) complexes with TMPA, TMPAE, BQPA, BPQA, and four dinuclear complexes $[[Cu_2(R\text{-}Xyl)(O_2)]^{2+}]$ employing dinucleating ligands where a *tridentate* pyridyl–alkylamino chelate is separated by a 5-substituted (R) *m*-xylyl spacer.[41] However, the room-temperature stability of all of these copper–dioxygen adducts is precluded by strongly negative reaction entropies, $\Delta S_1° = -123$ to -127 J K^{-1} mol^{-1} for the 1:1 adducts and $\Delta S_{12}° = -145$ to -250 J K^{-1} mol^{-1} for the 2:1 adducts. As an additional general trend within these series of complexes, more favorable enthalpies are compensated for by less favorable reaction entropies within the ranges cited.

While the kinetic and thermodynamic behavior of 1:1 O_2 binding to $[(D^1)Cu_2(EtCN)_2]^{2+}$ (**2a**) to form mixed-valent $[(D^1)Cu_2(O_2)(EtCN)]^{2+}$ (**2b**) and bis superoxo–copper(II) adduct $[(D^1)Cu_2(O_2)_2]^{2+}$ (**2b′**) follows that seen for $[(TMPAE)Cu(EtCN)]^+$ (**1a′**) → $[(TMPAE)Cu(O_2)]^+$ (**1b′**) and the others (e.g., complexes of TMPA and BQPA),[40] the 2:1 binding in the D^1 complex studied here stands in marked contrast. The intramo-

(76) Andrew, C. R.; McKillop, K. P.; Sykes, A. G. *Biochim. Biophys. Acta* **1993**, *1162*, 105–114.

lecular μ-peroxo complex $[(D^1)Cu_2(O_2)]^{2+}$ (**2c**) is formed from the 2:1 open intermediate $[(D^1)Cu_2(O_2)(EtCN)]^{2+}$ (**2b**) (eq 9). Entropic factors dominate the kinetics, favoring rapid depletion of **2a** and formation of **2c** over a wide range of temperatures. Both the kinetic activation entropies (for k_2, $\Delta S_2^{\ddagger} = -9$ J K^{-1} mol^{-1}, and for k_{on}, $\Delta S_{on}^{\ddagger} = -139$ J K^{-1} mol^{-1}) and overall thermodynamic entropy of formation (i.e., for K_1K_2, $\Delta S_{12}^{\circ} = -89$ J K^{-1} mol^{-1}) are considerably more favorable than what is seen in corresponding values for the mononuclear analogues TMPA, TMPAE, BQPA, BPQA,[40] and dinuclear $[Cu_2(R\text{-}Xyl)\text{-}(O_2)]^{2+}$,[41] vide supra. Thus, we succeeded in designing a structural analogue of $[\{(TMPA)Cu\}_2(O_2)]^{2+}$ (**1c**), as seen by the spectroscopic similarity of **2c** and **1c**, and we have overcome a sizable fraction of the large entropic handicap (i.e., $\Delta S_{12}^{\circ} = -220$ J K^{-1} mol^{-1} for **1c**) in the Cu_2-O_2 complexes formed from mononuclear precursors. However, our design of D^1 was not perfect, since it presents severe drawbacks in terms of the strain and weakened bonds of the derived Cu_2-O_2 moiety in $[(D^1)Cu_2(O_2)]^{2+}$ (**2c**), with a quite small $\Delta H_{12}^{\circ} = -35$ kJ mol^{-1}, compared to the $\Delta H_{12}^{\circ} = -81$ kJ mol^{-1} for **1c** formation [or even compared to $\Delta H_{12}^{\circ} = -50$ to -81 kJ mol^{-1}, the entire range we have observed for many other compounds (vide supra)]. As discussed, the strain manifests itself in (i) vis spectral shifts seen for the Cu_2-O_2 moiety, compared to **1c** or **1c'**; (ii) facilitated breaking of one Cu−O bond, i.e., favorable k_{-2} (eq 9) and associated $\Delta H_{-2}^{\ddagger}$ value compared to **1c** or **1c'**; and (iii) eventual complete conversion of $[(D^1)Cu_2(O_2)]^{2+}$ (**2c**) to *intermolecular* (peroxo)dicopper(II) $[\{(D^1)Cu_2(O_2)\}_n]^{2n+}$, which are less-strained oligomers.

These oligomers were also characterized by $\lambda_{max} = 529$ nm, a value much closer to that found in Cu_2-O_2 complexes formed from mononucleating ligands TMPA and TMPAE, namely, $[\{(TMPA)Cu\}_2(O_2)]^{2+}$ (**1c**) or $[\{(TMPAE)Cu\}_2(O_2)]^{2+}$ (**1c'**). The *intermolecular* nature of the Cu_2-O_2 moieties in these oligomers allows relief of steric strain, providing the driving force for their formation. A particularly stable cyclic trimer species $[\{(D^1)Cu_2(O_2)\}_3]^{6+}$ (**2d**) was identified; it possesses a ΔH_3° of formation (-51 kJ mol^{-1} on a per Cu_2-O_2 basis), making it less strained than its precursor **2c**, but still more strained than **1c** ($\Delta H_{12}^{\circ} = -81$ kJ mol^{-1}).

Thus, the Cu_2-O_2 μ-peroxo complex (or complexes) containing D^1 is (or are) in fact more stable than those found for mononucleating ligands TMPA or TMPAE. However, it is not the naively expected *intramolecular* species $[(D^1)Cu_2(O_2)]^{2+}$ (**2c**), but rather highly associated Cu_2-O_2 compounds formed in an *intermolecular* fashion, species that cannot possibly form with ligands like TMPA and TMPAE. A lesson from the present investigation is that there exists the possibility, or even the probability, that secondary rearrangements occur in reactions of dioxygen with dinuclear metal complexes, and that one must consider *intermolecularly* formed metal dioxygen species, in terms of analysis and interpretation of observed physical and spectroscopic properties, or reactivity patterns. In fact, evidence for such species for other copper[35,36,74,75] and iron[4] complexes already exists.

The future design of ligands that could lead to unstrained and stabilized structures is a challenge, not only to produce copper−dioxygen complexes which might have room-temperature stability but also to further amplify upon and test some of the notions or observations coming from this study. For example, how much entropy advantage can be generated in a dinucleating ligand, and are there other ways to do this? How much strain (i.e., loss of enthalpic stabilization) can one afford in order to favor the intramolecular μ-peroxo complex relative to other species? Knowledge of how to control or build in strain is of interest for tuning of dioxygen binding affinities, promoting enhanced reactivity (i.e., of peroxo−metal complexes) toward substrates, and in devising systems that could be catalytic (i.e., with turnover) in their O_2 reactions. Future investigations will address such issues, but will also include examination of synthetic variations of simpler mononuclear systems, to enhance our further basic understanding of how ligand electronic influences and steric factors control copper(I)/dioxygen reactivity.

Acknowledgment. We thank the National Institutes of Health (K.D.K., GM28962) and Swiss National Science Foundation (A.D.Z.) for support of this research. K.D.K. also thanks the National Science Foundation (CHE-9000471) for aid in the purchase of the X-ray diffractometer.

Supporting Information Available: Figures S1−S5 with ^{1}H NMR spectra of D^1 and $[(D^1)Cu_2(MeCN)_2]^{2+}$ (**2a**) at 298 and 230 K (S1), low-temperature benchtop UV−vis spectra at 193 K in propionitrile (S2), time dependence of the UV−vis spectra in the reaction of $[(TMPAE)Cu(MeCN)]^+$ (**1a'**) with O_2 (S3), absorbance vs time plots at 415 and 532 nm for the same reaction (S4), and an Eyring plot for k_{-3} (S5) (5 pages). This material is contained in many libraries on microfiche, immediately follows this article in the microfilm version of the journal, can be ordered from the ACS, and can be downloaded from the Internet; see any current masthead page for ordering information and Internet access instructions.

JA951933B